Title: A Cambrian spiny stem mollusc and the deep homology of lophotrochozoan scleritomes

Authors: Guangxu Zhang[1], Luke A. Parry[2*], Jakob Vinther[3], Xiaoya Ma[1,4*]

Affiliations:
[1]Yunnan Key Laboratory for Palaeobiology and MEC International Joint Laboratory for Palaeobiology and Palaeoenvironment, Institute of Palaeontology, Yunnan University, Kunming, China
[2]Department of Earth Sciences, University of Oxford, Oxford, UK
[3] Schools of Earth Sciences and Biological Sciences, University of Bristol, Bristol, UK
[4]Centre for Ecology and Conservation, University of Exeter, Penryn, UK

*Corresponding authors. Emails: luke.parry@earth.ox.ac.uk; x.ma2@exeter.ac.uk

Abstract: Molluscs encompass enormous disparity, including familiar clams and snails alongside less familiar aculiferans (chitons and vermiform aplacophorans) with complex multicomponent skeletons. Palaeozoic fossils trace crown molluscs to forms exhibiting a combination of biomineralised shells and sclerites (e.g scales, spines and spicules). We describe a shell-less, Cambrian stem mollusc, *Shishania aculeata* gen. et sp. nov., with conical, hollow chitinous sclerites and a smooth girdle, broad foot, and mantle cavity. The sclerites have a microstructure of narrow canals consistent with the impressions of chaetal microvilli found in annelids and brachiopods. *Shishania* sclerites provide a morphological stepping stone between typical chaetae (chitinous bristles) and the external organic part of aculiferan sclerites that encloses a mineralised body. This discovery reinforces a common origin of lophotrochozoan chaetae and the biomineralized aculiferan sclerites, suggesting the mollusc ancestor was densely covered with hollow chitinous chaetae.

One-Sentence Summary: New fossils reveal the origin of molluscan skeletons

Introduction

The extant mollusc lineages diversified rapidly during the early Cambrian (*1, 2*), making it difficult to infer their phylogenetic relationships and early evolutionary history. Recently, a combination of the study of early fossils and an increasingly well-resolved phylogenomic framework for molluscan relationships suggest a single-shelled molluscan common ancestor, with a deep split between molluscs with single or paired shells (Conchifera) and those with multi-element scleritomes made up of small sclerites, such as scales, spines and spicules in aculiferans. Extant aculiferan molluscs possess either 8, serially repeated shells as in chitons, or in Aplacophora lack shells altogether, with the shell-less condition arising from chiton-like, 8 shelled ancestors (*1, 3-5*).

Stem-group molluscs from the Cambrian are represented by forms with sclerites exhibiting a microstructure like that of annelid chaetae (i.e. *Wiwaxia (6)*) alongside the naked *Odontogriphus* (*7*). Whether the multi-element *Wiwaxia* scleritome is homologous with that of extant aculiferans is unclear, and so it is unknown if an aculiferan-like scleritome was present in the molluscan ancestor. *Wiwaxia* was previously interpreted as a stem or crown annelid as opposed to a mollusc (*8*) on the basis of the microvillar, tubular microstructure preserved within its distinctive sclerites (*6*) prior to the detailed investigation of its radula (*9*)

Here we describe a new early Cambrian (Stage 4, ~514-509 million years old), shell-less, armoured animal, *Shishania aculeata* gen. et sp. nov., that has conical, organic sclerites distributed across the dorsum. The ventral surface consists of a smooth girdle that lacks sclerites, separated from a broad foot by a narrow mantle cavity. Like sclerites of some early aculiferans (e.g. halkieriids (*10*)), these sclerites are hollow. The organic outer envelope of the sclerite additionally preserves a fine microstructure of narrow longitudinal striations consistent with the impressions of microvilli, typical of the chitinous appendages (e.g. chaetae) observed in *Wiwaxia (6),* annelids (*11*), lophophorates (*12*) and some molluscs (*13*). Our phylogenetic analyses place *Shishania aculeata* in the molluscan stem-group, crownward of *Wiwaxia,* indicating the presence of an organic scleritome derived from chaeta-like sclerites deep in the ancestry of molluscs. The hollow, non-mineralised sclerites of *Shishania* provide morphological evidence that bridge the evolutionary gap between the solid, leaf-like scales of *Wiwaxia* and the hollow portion of the sclerites of aculiferans that encloses a biomineralized body. This reinforces the case for the chaetae of annelids and brachiopods (and their tommotiid stem lineages (*12*)) sharing a common origin with the biomineralized sclerites of aculiferan molluscs. Along with evidence from fossil annelids and stem lophophorates (tommotiids (*12*)), this suggests that a chitinous, organic scleritome has an ancient origin in Lophotrochozoa and has been reduced, lost, biomineralized or otherwise elaborated in different lineages and that the mollusc ancestor was densely covered with chitinous sclerites that share a common origin with annelid chaetae.

Systematic Palaeontology

Mollusca Linnaeus, 1758

Shishania aculeata gen. et sp. nov.

Etymology: *Shishan* refers to Shishan Zhang, for his outstanding contributions to the study of early Cambrian strata and fossils in eastern Yunnan; *aculeata* (Latin), having spines, prickly.

Holotype: YKLP 11500 (YKLP, Yunnan Key Laboratory for Palaeobiology) (Fig. 1, A and B, and fig. S1).

LSID: urn:lsid:zoobank.org:pub:A0A31BE4-D8F9-4E99-83E1-C3377D075D14

Paratypes: YKLP 11501 (Figs. 2 and 3, H to K, and fig. S7), YKLP 11502 (Fig. 1, E and F), YKLP 11503 (fig. S4, A to C), YKLP 11504 (Fig. 3, A to F), YKLP 11505 (fig. S3, G to I), YKLP 11526 (fig. S4, D to H), YKLP 11527 (Fig. 1, G and H, and fig. S5), YKLP 11535 (fig. S3, A to F).

Referred material: YKLP 11528 (fig. S2G), YKLP 11529 (fig. S2A), YKLP 11530 (fig. S2B), YKLP 11531 (fig. S2C), YKLP 11532 (fig. S2E), YKLP 11533 (fig. S2F), YKLP 11534 (fig. S2H), YKLP 11536 (fig. S2D), YKLP 11537 (fig. S2I).

Horizon and locality: All specimens are derived from the lower part of the Wulongqing Formation, *Megapalaeolenus* Zone (Cambrian Series 2, Stage 4) in Fuming County, Kunming city, eastern Yunnan Province, China.

Diagnosis: A flattened, bilaterally symmetrical animal covered with dorsal hollow, conical sclerites embedded within a thick extra-cellular matrix (mantle). Sclerites possess a microstructure of narrow (~90-350 nm), hollow striations that parallel the growth axis. The ventral side of the body lacks sclerites and is divided into a peripheral girdle/ventral mantle, a mantle cavity, and a muscular foot that occupies half of the body width.

Description: The holotype, YKLP 11500 (Fig. 1, A to C and fig. S1), is a complete specimen preserved in dorsal view. It is ~27 mm in length and ~21 mm in width (excluding sclerites). The dorsal surface is densely covered in sclerites, at a density of ~120 sclerites per cm^2. The sclerites vary from 90-170 µm in length and have apical angles of 28-41°. Additional information on the body plan and anatomy of *Shishania aculeata* is given by specimens in dorsal (figs. S1 and S2, A to C, and E), ventral (figs. S2G and S3) and lateral/oblique/distorted views (Fig. 1, E and G, figs. S4 and S5). The specimens range from 13 mm to in excess of 60 mm long and 13 mm to 40 mm in width.

YKLP 11502 is preserved in an oblique/lateral view (Fig. 1E), with the margin of the body readily visualised using elemental maps for iron and sulphur (Fig. 1F, and fig. S6). This lateral view and other lateral/oblique specimens (fig. S4) demonstrate that the body was dorsoventrally flat in life.

The sclerites are straight sided cones with sharp pointed apices (apical angle $\bar{x}$=36.46°, σ=5.06). Oblique views reveal hollow bases (Fig. 2A, and fig. S1, E and F). This hollow morphology is further indicated by dark outlines at the sclerite margins, where the carbon films have been thickened by compaction, but more diffuse sclerite interiors, suggesting that they were not thickly sclerotised and instead were formed of a relatively thin organic envelope. This mode of preservation precludes original mineralisation of the sclerites, such as in aragonite. Taxa that were originally mineralised, such as trilobites or hyoliths, are preserved without their original biominerals but with substantial relief, indicating demineralisation happened late relative to compaction of the fossil specimens. Faint transverse annulations are present, which are visible in both lateral (Fig. 2A) and dorsal (Fig. 2B) views, although in the latter they are likely enhanced by compaction. A sclerite that is broken and torn at its base (Fig. 2C) further illustrates that the sclerites were not heavily sclerotised in their interior but were a relatively thin cuticle. The sclerites are preserved as organic films (Fig. 2, D and E), which were sometimes subsequently partially pyritized (Fig. 3J). Where preserved organically, scanning electron microscopy reveals a fabric of longitudinal striations that is distinct from the sedimentary fabric in the surrounding matrix (Fig. 2, F and G, and fig. S6). These striations consist of longitudinal striations that parallel the growth axis of the sclerite and vary between 57 and 345 nm in diameter ($\bar{x}$=193.4nm.) (Fig. 2H, and figs. S7 and S8). The sclerites are embedded in a tissue preserved as a material that was originally pyritised, shown by enrichment in iron and sulfur (Fig. 3J), the latter of which has been lost to weathering to a varying degree. In specimens preserved in ventral view the sclerite bases can be seen as concave deformation relative to the plane on which the fossil is preserved (Figs. 1H and 3F, and fig. S3, D and E) where they have been obscured by this underlying tissue. This thickened dorsal tissue resembles a mantle, thickened with extracellular matrix, such as the girdle in chitons. The girdle extends to the periphery of the ventral portion (Fig. 3, A to C, and fig. S3, A to E), where it lacks sclerites and was heavily pyritised.

Ventral (Fig. 3, A and B, and fig. S3), lateral/oblique (Fig. 1, E and G, and fig. S4) and dorsal views where the specimen has split through different body regions, inferred by the relative superposition of the body regions revealed in different specimens (Fig. 3, H and L) reveal an entirely naked ventral surface (Fig. 3, A and F), that is separated into three zones, each with a distinctive morphology, comparable with the ventral surface of extant polyplacophorans (Fig 3G). Sclerites project from the lateral margin of the body (Fig. 3, A and D), with the periphery of the ventral surface surrounded by a smooth girdle (Fig. 3, and figs. S3 and S5). Specimen YKLP 11504 is exposed in ventral view and shows clear preservation of the foot (Fig. 3, A and B, and fig. S3). This is particularly evident in reflectance transformation imaging, demonstrating the foot occupies ~50% of the width of the body and is separated from the lateral girdle by a steep break of slope, which indicate the intervening mantle cavity between the margins of the foot and the ventral mantle region which is devoid of sclerites (Fig. 3, A to C, and fig. S3). A dorsal specimen of *S. aculeata* that split at different planes also reveals a smooth peripheral girdle on the ventral side of the body, as well as an internal cavity preserved in both relief and a lighter coloured mineral than the surrounding mantle tissues (Fig. 3, H to K). This style of preservation is comparable to the largest, specimen of *Calvapilosa* preserving soft tissues (1). Both the mantle cavity and the girdle are distinct from the dorsal tissues in x-ray fluorescence maps for sulfur and iron (Fig. 3J). One specimen in dorsal view shows a feature region with an anterior-posterior trajectory that is devoid of sclerites and texturally different from the surrounding mantle tissue, that likely represents the gut (Fig. 3, H to K) A summary of the body regionalisation based on all the available specimens is shown as a cross section in Figure 3L.

An anteriorly incomplete digestive tract has been found in one specimen (YKLP 11501) (e.g. Fig. 3, H, I and K). This structure is interpreted as a gut due to its distinct anterior-posterior trajectory, differentiated morphology and topographic relationships to the overlying tissues that are interpreted as the external mantle and sclerites. It is identified in normal light imaging (Fig. 3H), which also delineates the superposition of the different tissues as well as a lack of sclerites and a difference in texture compared with the surrounding tissues. No internal structures associated with the anterior digestive tract (i.e. a jaw apparatus or radula) were observed in any of our specimens, or such structures may be obscured by the dorsal scleritome. For comparison, mouth parts are visible in fewer than a third of *Wiwaxia corrugata* specimens from the Burgess Shale (*9*) (which is known from hundreds of specimens) and consequently we remain agnostic regarding the presence/absence of a radula in *Shishania.*

Phylogenetic analysis and ancestral state reconstruction

Shishania is recovered as a stem-group mollusc in our phylogenetic analysis, recovering a topology that is similar to previous analyses of the datasets from which ours is derived (*1, 12, 14*). *Shishania* is recovered in a polytomy with *Odontogriphus* that subtends the molluscan crown relative to *Wiwaxia* (Fig. 4A). These results do not vary with the exclusion of the controversial Ediacaran taxon *Kimberella (15)* or the use of topological constraints (figs. S8 and S9). Ancestral state reconstruction recovers a mollusc crown ancestor with a single shell plate and a chitinous scleritome made of hollow, unmineralised, conical sclerites that are spatially separated from each other over the dorsal body wall (Fig. 4) that evolved within the mollusc stem-group (Fig. 4).

Discussion

Shishania aculeata gen. et sp. nov. is a dorsoventrally flattened bilaterian with a thick, sclerite covered mantle, a smooth ventral girdle, a peripheral mantle cavity and a distinct foot (Fig. 4). This combination of characters is only present in molluscs. While many bilaterians have a ciliary gliding sole (particularly within Lophotrochozoa/Spiralia), only molluscs have evolved a distinct organ that is separated from the dorsal surface by a mantle cavity.

Chitinous elements with tubular internal canals are widespread among lophotrochozoans, specifically trochozoans. They occur in brachiopods (along the mantle periphery and in clusters on the dorsal side of their larvae (*16*)), on the parapodia of annelids (*17*) and in some extinct and extant molluscs (*18-20*), and in the gizzard of bryozoans (*21*). The tubular canals form as the chitinous matrix is secreted by cells densely covered with microvilli and have a diameter of ~50nm-1000 nm. All of these structures (and likewise the conical sclerites of *Shishania*) are secreted with new material deposited at their base, such that the apex formed first. This deposition process imparts a distinctive honeycomb texture of tubular canals in transverse cross section, that appear as parallel striations in longitudinal views, providing means to identify chitinous sclerites and chaetae in fossil taxa (*6*). Ultrastructural (*22*), phylogenetic (*23, 24*) and evidence from evo-devo (*25*) suggests that chaetae are homologous across all these trochozoan taxa. Their widespread occurrence in extinct taxa (*6, 12*) has prompted much debate about the affinities of certain fossils and the nature of the ancestral trochozoan (*8, 11, 12, 26, 27*).

The most common form of chitinous appendage amongst trochozoans are slender, capillary chaetae in fascicles (bundles), which are present in many annelids, brachiopod larvae, stem lophophorates (*12*), and in extinct (*Pelagiella (20)*) and extant conchiferan molluscs (i.e. juvenile octopuses (*18*)). In aculiferan molluscs (i.e. chitons and aplacophorans), some forms exhibit chitinous hairs (*28*) with the same microvillar microstructure. Aculiferan sclerites are otherwise biomineralized, but nevertheless retain a chitinous envelope that retains the distinctive microstructure of impressions formed by secretion by microvilli (*19*). Aculiferan sclerites typically constrict to a basal stalk, and unlike the typical bundles/fascicles of chaetae present in annelids and *Wiwaxia* they are dispersed across the body wall, forming a dense scleritome. Such a scleritome is present in sachitids, such as the iconic taxon *Halkieria*, and a seemingly intermediate scleritome in *Wiwaxia,* where solid organic sclerites in serialised rows with a hollow stalk are present in bundles (*6, 11, 26*). These elaborate scleritomes and the presence of paired shells in *Halkieria* prompted hypotheses that these taxa were intermediate between annelids and brachiopods (*8*), but the presence of radulae with serialised tooth rows, rachidian (median) teeth in *Wiwaxia* and the Ordovician sachitid *Calvapilosa* has placed these taxa more firmly on the molluscan and aculiferan stem lineages respectively (*1*).

The middle Cambrian stem-group mollusc *Odontogriphus* from the Burgess Shale preserves evidence of a foot, mantle cavity and a radula with only 3-5 tooth rows like that of *Wiwaxia*, but was apparently naked, lacking an extensive scleritome (*7*) although it may have fine chaetal hairs that remain undocumented. This raises two possibilities for the origin of the aculiferan scleritome. Either it was inherited from the molluscan stem-group and subsequently lost in conchiferan molluscs (*1, 29*) or *Wiwaxia* and the aculiferan total group independently acquired a dense, dorsal scleritome. While *Shishania*'s scleritome with dispersed sclerites and absence of a shell could be interpreted as indicative of an aplacophoran affinity*,* fossil aplacophorans from the Silurian demonstrate that this class retained seven dorsal shells after reduction of the foot (*3-5, 30*) as well as evidence from a footless, Late Ordovician stem aplacophoran that retained eight shell plates (*4*). Unlike in fossil and extant Aplacophora the

foot and the peripheral mantle cavity are well-developed in *Shishania,* resembling those of chitons and monoplacophorans. This therefore conflicts with affinities with the aplacophoran total group, which appeared to have diverged from a common ancestor with chitons around the Cambrian/Ordovician boundary (*30*). While the sclerites of *Shishania* are hollow (although most likely filled with living tissue in life), like those of some aculiferans, they do not constrict basally to form a stalk, and their low relief is consistent with being unmineralized. The absence of a discrete shell is suggestive of a position outside the molluscan crown-group, as both the aculiferan and conchiferan ancestor are inferred to have possessed a single shell plate, which is present in the stem lineage of Aculifera and stem lineages of all of the conchiferan classes (*1*). While the precise origins of this shell remain unclear, developmental genetic data indicate deep homology of shells and chaetae (*25*), which is consistent with the presence of early Cambrian sachitids (e.g. *Siphogonuchites*) whose shells were formed of merged sclerites (*Maikhanella*) (*31, 32*), which could therefore feasibly be stem group molluscs, consistent with their older occurrence than unequivocal conchiferans and *Halkieria* in the *Purella* Biozone (*33*). The scleritome of *Shishania* consisting of dispersed hollow organic sclerites, and its inferred position on the molluscan stem, provide direct evidence that the aculiferan scleritome has a deep origin and has been lost in conchiferan molluscs. Additionally, the fine structure of *Shishania*'s sclerites is consistent with chitin secreted by microvilli. The sclerites of aculiferan molluscs have a similarly secreted, organic outer envelope that houses a mineralised body (*13*) and so the hollow unmineralized sclerites of *Shishania* provide a long awaited morphological stepping stone between more typical chaetae and molluscan sclerites as portrayed in our phylogenetic analysis and ancestral state reconstruction (Fig. 4A). These results complement and bolster a growing body of evidence from early annelids and stem-group lophophorates (camenellan tommotiids) (*12*) that a dense covering of chaetae with a inferred protective function was shared by the common ancestor of multiple phyla within Lophotrochozoa, which constitute one of the most morphologically disparate groups of animals alive today.

References and Notes

1. J. Vinther, L. Parry, D. E. G. Briggs, P. Van Roy, Ancestral morphology of crown-group molluscs revealed by a new Ordovician stem aculiferan. *Nature* **542**, 471 (2017).
2. H. Song *et al.*, Scaphopoda is the sister taxon to Bivalvia: Evidence of ancient incomplete lineage sorting. *Proceedings of the National Academy of Sciences* **120**, e2302361120 (2023).
3. M. D. Sutton, D. E. G. Briggs, D. J. Siveter, D. J. Siveter, J. D. Sigwart, A Silurian armoured aplacophoran and implications for molluscan phylogeny. *Nature* **490**, 94-97 (2012).
4. M. D. Sutton, J. D. Sigwart, A chiton without a foot. *Palaeontology* **55**, 401-411 (2012).
5. M. D. Sutton, D. E. G. Briggs, D. J. Siveter, D. J. Siveter, An exceptionally preserved vermiform mollusc from the Silurian of England. *Nature* **410**, 461-463 (2001).
6. N. J. Butterfield, A reassessment of the enigmatic Burgess Shale fossil *Wiwaxia corrugata* (Matthew) and its relationship to the polychaete *Canadia spinosa* Walcott. *Paleobiology* **16**, 287-303 (1990).
7. J.-B. Caron, A. Scheltema, C. Schander, D. Rudkin, A soft-bodied mollusc with radula from the Middle Cambrian Burgess Shale. *Nature* **442**, 159-163 (2006).

8. S. Conway Morris, J. S. Peel, Articulated halkieriids from the Lower Cambrian of North Greenland and their role in early protostome evolution. *Philosophical Transactions of the Royal Society of London B: Biological Sciences* **347**, 305-358 (1995).
9. M. R. Smith, Mouthparts of the Burgess Shale fossils *Odontogriphus* and *Wiwaxia*: implications for the ancestral molluscan radula. *Proceedings of the Royal Society B: Biological Sciences*, rspb20121577 (2012).
10. J. Vinther, The canal system in sclerites of Lower Cambrian Sinosachites (Halkieriidae: Sachitida): significance for the molluscan affinities of the sachitids. *Palaeontology* **52**, 689-712 (2009).
11. D. Eibye-Jacobsen, A reevaluation of *Wiwaxia* and the polychaetes of the Burgess Shale. *Lethaia* **37**, 317-335 (2004).
12. J. Guo *et al.*, A Cambrian tommotiid preserving soft tissues reveals the metameric ancestry of lophophorates. *Current Biology* **32**, 4769-4778. e4762 (2022).
13. F. P. Fischer, W. Maile, M. Renner, Die Mantelpapillen und Stacheln vonAcanthochiton fascicularis L.(Mollusca, Polyplacophora). *Zoomorphologie* **94**, 121-131 (1980).
14. H. Chen, Parry, L.A., Vinther, J., Zhai, D., Xianguang, H., Ma, X. A A Cambrian crown annelid reconciles phylogenomics and the fossil record. *Nature* **583**, 249-252 (2020).
15. M. A. Fedonkin, B. M. Waggoner, The Late Precambrian fossil Kimberella is a mollusc-like bilaterian organism. *Nature* **388**, 868-871 (1997).
16. C. Nielsen, The development of the brachiopod *Crania* (*Neocrania*) anomala (OF Müller) and its phylogenetic significance. *Acta Zoologica* **72**, 7-28 (1991).
17. R. A. Merz, S. A. Woodin, Polychaete chaetae: Function, fossils, and phylogeny. *Integrative and Comparative Biology* **46**, 481-496 (2006).
18. S. L. Brocco, R. M. O'Clair, R. A. Cloney, Cephalopod integument: the ultrastructure of Kölliker's organs and their relationship to setae. *Cell and Tissue Research* **151**, 293-308 (1974).
19. F. P. Fischer, W. Maile, M. Renner, The mantle papillae and the spines in *Acanthochiton fascicularis* L.(Mollusca, Polyplacophora). *Zoomorphologie* **94**, 121-131 (1980).
20. R. D. Thomas, B. Runnegar, K. Matt, *Pelagiella exigua*, an early Cambrian stem gastropod with chaetae: lophotrochozoan heritage and conchiferan novelty. *Palaeontology* **63**, 601-627 (2020).
21. D. P. Gordon, The Resemblance of Bryozoan Gizzard Teeth to “Annelid-like” Setae. *Acta zoologica* **56**, 283-289 (1975).
22. C. Lüter, Ultrastructure of larval and adult setae of Brachiopoda. *Zoologischer Anzeiger* **239**, 75-90 (2000).
23. C. W. Dunn *et al.*, Broad phylogenomic sampling improves resolution of the animal tree of life. *Nature* **452**, 745-749 (2008).
24. F. Marlétaz, K. T. Peijnenburg, T. Goto, N. Satoh, D. S. Rokhsar, A new spiralian phylogeny places the enigmatic arrow worms among gnathiferans. *Current Biology* **29**, 312-318. e313 (2019).
25. S. M. Schiemann *et al.*, Clustered brachiopod Hox genes are not expressed collinearly and are associated with lophotrochozoan novelties. *Proceedings of the National Academy of Sciences*, 201614501 (2017).
26. Z. Zhang, M. R. Smith, D. Shu, New reconstruction of the *Wiwaxia* scleritome, with data from Chengjiang juveniles. *Scientific reports* **5**, (2015).

27. F. Zhao *et al.*, Orthrozanclus elongata n. sp. and the significance of sclerite-covered taxa for early trochozoan evolution. *Scientific reports* **7**, 16232 (2017).
28. E. M. Leise, R. A. Cloney, Chiton integument: ultrastructure of the sensory hairs of Mopalia muscosa (Mollusca: Polyplacophora). *Cell and tissue research* **223**, 43-59 (1982).
29. M. R. Smith, Ontogeny, morphology and taxonomy of the soft-bodied Cambrian 'mollusc' *Wiwaxia*. *Palaeontology* **57**, 215-229 (2014).
30. J. Vinther, E. A. Sperling, D. E. G. Briggs, K. J. Peterson, A molecular palaeobiological hypothesis for the origin of aplacophoran molluscs and their derivation from chiton-like ancestors. *Proceedings of the Royal Society of London B: Biological Sciences* **279**, 1259-1268 (2012).
31. S. Bengtson, The cap-shaped Cambrian fossil Maikhanella and the relationship between coeloscleritophorans and molluscs. *Lethaia* **25**, 401-420 (1992).
32. Y. n. Zhang *et al.*, New Early Cambrian Maikhanellids (Mollusca) from Zhangjiagou Section, South Shaanxi, China. *Acta Geologica Sinica-English Edition* **96**, 440-446 (2022).
33. A. Kouchinsky *et al.*, Terreneuvian stratigraphy and faunas from the Anabar Uplift, Siberia. *Acta Palaeontologica Polonica* **62**, 311-440 (2017).
34. H. Luo, S. Hu, L. Chen, S. Zhang, Y. Tao, *Early Cambrian Chengjiang fauna from Kunming region, China*. (Yunnan Science and Technology Press, 1999).
35. F. Ponchio, M. Corsini, R. Scopigno, RELIGHT: A compact and accurate RTI representation for the web. *Graphical Models* **105**, 101040 (2019).
36. G. Palma, M. Corsini, P. Cignoni, R. Scopigno, M. Mudge, Dynamic shading enhancement for reflectance transformation imaging. *Journal on Computing and Cultural Heritage (JOCCH)* **3**, 1-20 (2010).
37. E. Tilic, T. Herkenrath, G. Kirfel, T. Bartolomaeus, The cellular 3D printer of a marine bristle worm—chaetogenesis in Platynereis dumerilii (Audouin & Milne Edwards, 1834)(Annelida). *Cell and Tissue Research* **391**, 305-322 (2023).
38. L. Orrhage, Light and electron microscope studies of some brachiopod and pogonophoran setae: With a discussion of the "annelid seta" as a phylogenetic-systematic character. *Zeitschrift für Morphologie der Tiere* **74**, 253-270 (1973).
39. L. A. Parry, G. D. Edgecombe, D. Eibye-Jacobsen, J. Vinther, The impact of fossil data on annelid phylogeny inferred from discrete morphological characters. *Proceedings of the Royal Society B* **283**, 20161378 (2016).
40. F. Ronquist *et al.*, MrBayes 3.2: efficient Bayesian phylogenetic inference and model choice across a large model space. *Systematic Biology* **61**, 539-542 (2012).
41. L. Parry, J.-B. Caron, *Canadia spinosa* and the early evolution of the annelid nervous system. *Science Advances* **5**, eaax5858 (2019).
42. L. A. Parry, G. D. Edgecombe, D. Sykes, J. Vinther, Jaw elements in Plumulites bengtsoni confirm that machaeridians are extinct armoured scaleworms. *Proceedings of the Royal Society B* **286**, 20191247 (2019).
43. H. Sun *et al.*, Hyoliths with pedicles illuminate the origin of the brachiopod body plan. *Proceedings of the Royal Society B: Biological Sciences* **285**, 20181780 (2018).

Acknowledgments:

We thank H. Zhang, L. Jiang, and Z. Yang for support in field collection, P. Cong, S. Zhang for providing RTI equipment, X. Lei for SEM technical support, and M. Cawthorne for artistic reconstructions shown in Fig. 4 and thumbnail images in figs. S9 and S10.

Funding: Yunnan Fundamental Research Projects grant no. 202301BF07001-021 (XM)

NERC Independent Research Fellowship grant no. NE/W007878/1 (LAP)

Author contributions: All authors made equal contributions to interpreting the fossil specimens and their anatomy. GZ collected and photographed all specimens, including SEM and RTI imaging. LAP and GZ made the figures and performed the phylogenetic analyses. JV collated and measured microvillar microstructure. XM secured funding and provided project administration and supervision. LAP and JV wrote the initial manuscript with subsequent input from all other authors.

Competing interests: We declare no competing interests.

Data and materials availability: All data analysed in this paper are available as part of the published paper or supplementary information. All fossil material described in this study is deposited in the collections of the Yunnan Key Laboratory for Palaeobiology, Yunnan University, Kunming, China. This fossil material is deposited with accession numbers YKLP11501-11505 and YKLP11526-11537. The phylogenetic dataset and commands and topological constraints necessary to run the MrBayes analyses are included as NEXUS formatted files. The nomenclatural acts in this publication have been registered at ZooBank with the following LSID: urn:lsid:zoobank.org:pub:A0A31BE4-D8F9-4E99-83E1-C3377D075D14. RTI 351 datasets are deposited at Dryad DOI: 10.5061/dryad.tb2rbp08n

Supplementary Materials

Materials and Methods

Supplementary Text

Figs. S1 to S9

Tables S1

References (*29-38*)

Data S1 to S2

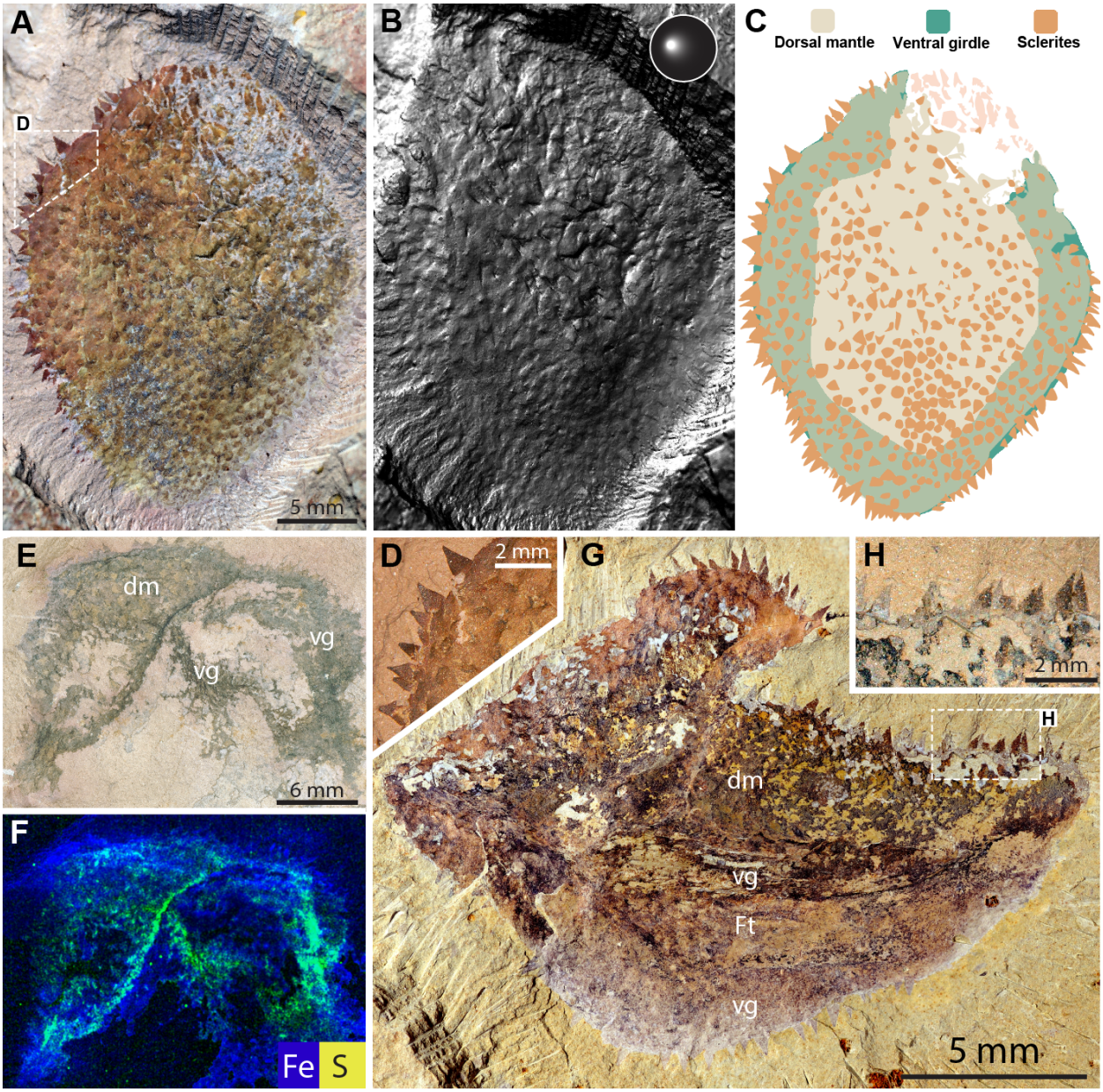

Fig. 1. Gross morphology of *Shishania aculeata* gen. et sp. nov. (**A** to **D**) Holotype YKLP 11500, a complete specimen in dorsal view. In (A), the image was taken under normal light. In (B**),** a Reflectance Transformation Image (RTI) rendered using specular enhancement to enhance topography, particularly the ventral girdle. In (C)**,** interpretive illustration, showing sclerites and body outline and topographic information from (B). In (D), details of anterior sclerites. (**E** and **F**) Specimen YKLP 11502, in oblique view, showing both dorsal and ventral anatomy. In (E), the image was taken under normal light. In (F)**,** the elemental map from XRF analysis highlights the body outline and ventral anatomy (Blue is iron, yellow is sulfur, and the overlap between these is green and consistent with the presence of pyrite). (**G** and **H**) Specimen YKLP 11527, anteriorly distorted specimen, showing the ventral region in oblique view. In (G), the entire specimen, showing different regions of the dorsal mantle, ventral girdle, and foot. In (H), a close-up of the sclerites at the body margin. Abbreviations: dm - dorsal mantle, vg - ventral girdle, Ft - foot.

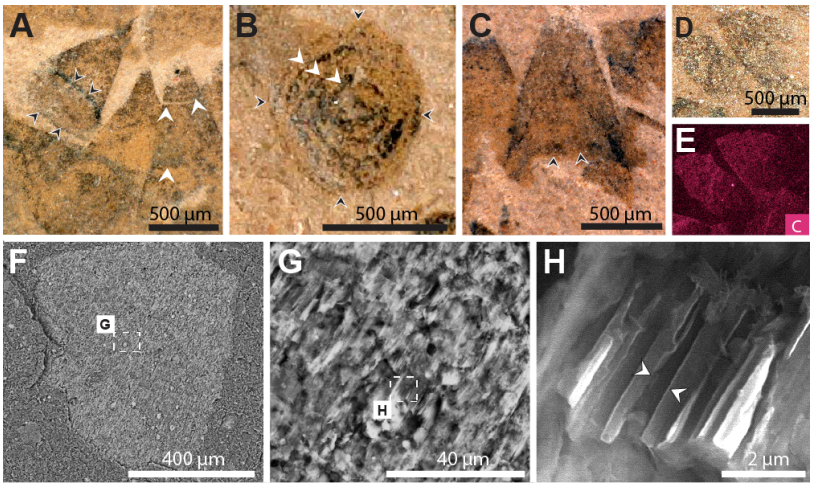

Fig. 2. Sclerites from specimen YKLP 11501 of *Shishania aculeata* gen. et sp. nov. (**A**) Sclerites showing conical shape, the outline of a circular base (black-filled arrowheads), and weak transverse ornamentation (white arrowheads). (**B**) Sclerites in dorsal view, showing circular outline (black-filled arrowheads) and concentric ornamentation (white arrowheads). (**C**) Sclerites showing a possible torn base and hollow interior. (D and E) Elemental analysis of sclerites. In (D), sclerites imaged under normal light. In (E), a carbon map from XRF analysis of the same region shown in (D). (**F**) Scanning Electron Microscope (SEM) image of the sclerites, showing a distinct parallel linear fabric within the sclerite that is distinct from that of the matrix. (**G**) Detail of longitudinal striations in the sclerites shown in (F). (**H**) Close-up of longitudinal sclerite microstructural fabric shown in (G), showing longitudinal hollow striations within the sclerite wall (white-filled arrowheads). Black-filled arrowheads in **A-C** indicate sclerite bases, white arrowheads in **A,B** indicate transverse ornament and white-filled arrowheads in **H** delineate the concave area denoting an individual tubule within a sclerite.

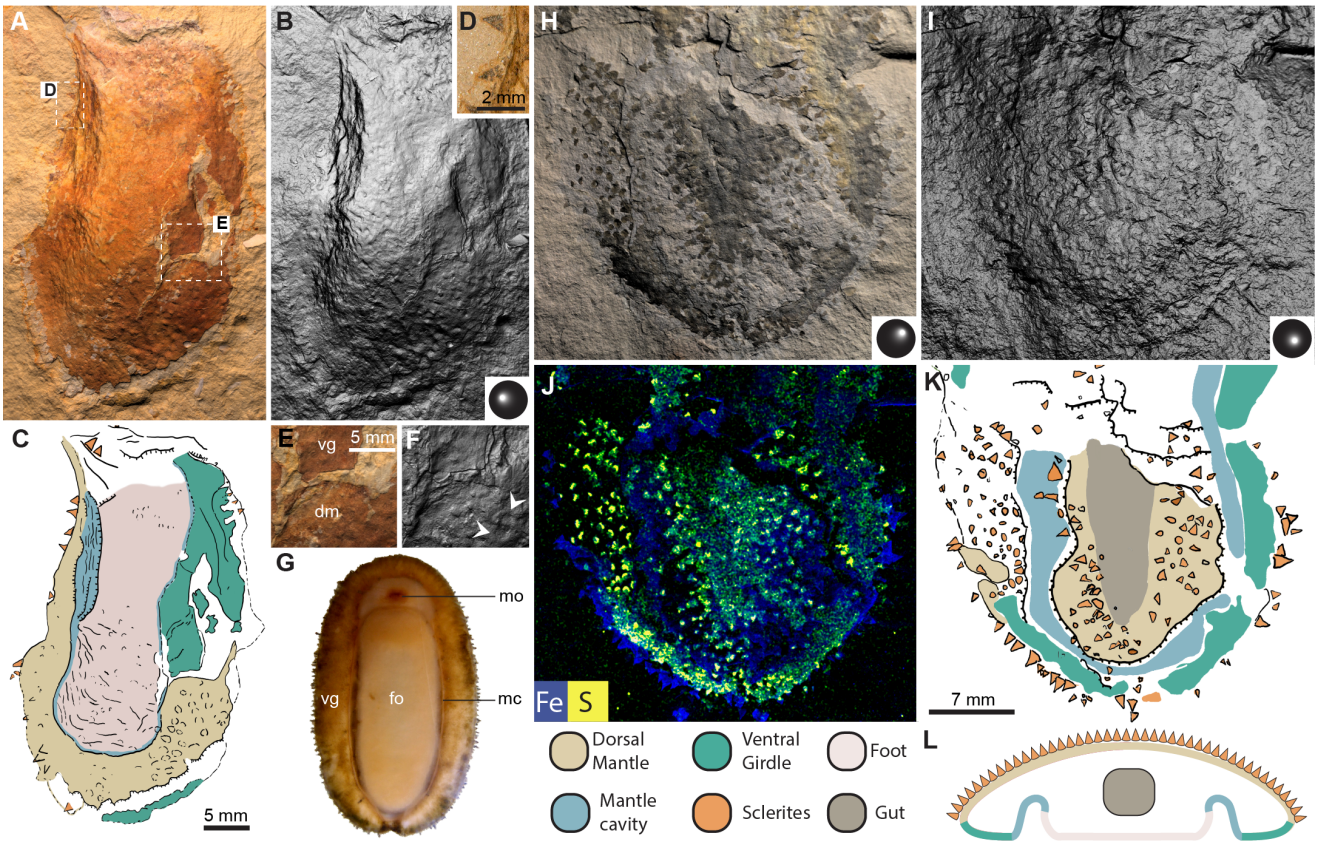

Fig. 3. Molluscan characters preserved in *Shishania aculeata* gen. et sp. nov. (**A** to **F**) Specimen YKLP 11504, an anteriorly incomplete specimen preserved in ventral view, showing the foot and ventral girdle. In (A), the image taken under normal light. In (B)**,** an RTI image rendered using specular enhancement to enhance relief. In (C), interpretive illustration based on information shown in (A) and (D). In (D), sclerites at the body margin. In (E)**,** preservation of the ventral girdle and dorsal mantle where the specimen has split partially through the dorsal and ventral surfaces. In (F)**,** the same region as in (E), an RTI image rendered using specular enhancement to highlight relief, white arrowheads indicate sclerite bases that are preserved as concave deformation through the dorsal mantle. (**G**) Extant chiton (*Mopalia muscosa*) in ventral view alive and imaged through a glass plate. (**H** to **K**) Specimen YKLP 11501, a posterior fragment preserved in dorsal view. In (H), an RTI image rendered using diffuse gain. In (I), an RTI image of the same region shown in (H), rendered using specular enhancement to highlight the relief of different regions of the body and separation into distinct morphological zones. In (J)**,** an elemental map from XRF analysis, showing Iron and Sulfur (blue is iron, yellow is sulfur, and the overlap between these is green and consistent with the presence of pyrite). In (K), the interpretive drawing of body regionalization based on (H) to (J). (**L**) Reconstruction of the transverse cross section of *Shishania aculeata* based on observations of multiple specimens. Abbreviations: vg - ventral mantle, dm - dorsal mantle, mo - mouth, fo - foot, mc - mantle cavity.

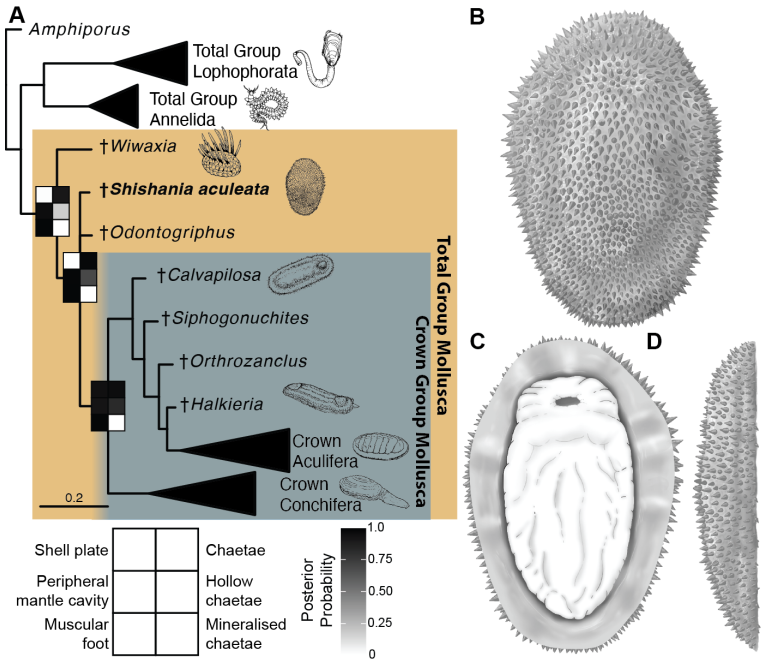

Fig. 4. Phylogenetic position of *Shishania aculeata* gen. et sp. nov., ancestral states for select nodes and life reconstruction. (**A**) Majority rule consensus tree of the posterior sample of a Bayesian analysis (mk model), note that some clades are collapsed for clarity. See figs. S8 and S9 for full topologies from the phylogenetic analyses. Grid plots at nodes are posterior probabilities and topology shown is from the unconstrained analysis without *Kimberella.* The scale bar is in units of the expected number of substitutions per site. (**B** to **D**) Life reconstruction of *Shishania aculeata* in dorsal (B), lateral (C) and ventral view (D), note that reconstruction of the oral region is speculative.

Science
AAAS

Supplementary Materials for

Title: A Cambrian spiny stem mollusc and the deep homology of lophotrochozoan scleritomes

Authors: Guangxu Zhang[1], Luke A. Parry[2*], Jakob Vinther[3], Xiaoya Ma[1,4*]

*Corresponding authors. Emails: luke.parry@earth.ox.ac.uk; x.ma2@exeter.ac.uk

The PDF file includes:

Materials and Methods

The specimens were collected from a stockyard where the Kun-Shang Highway was being built in 2019, in Fuming County, eastern Yunnan Province, China. Therefore, no collection permit was required. All specimens figured in this work were collected by Guangxu Zhang & Zhixin Yang between 2019 and 2022. This fossil site belongs to the lower part of the Wulongqing Formation, the age of which is constrained to Cambrian Series 2, Stage 4 (~514-509 Ma) based on trilobite biostratigraphy, with fossil bearing levels occurring in the *Megapalaeolenus* biozone (*34*). All specimens are housed at the Yunnan Key Laboratory for Palaeobiology, Yunnan University, Kunming, China. Eighteen specimens were studied in total with accession numbers YKLP11501-11505 and YKLP11526-11537.

Specimens were photographed with a Keyence VHX 6000 digital microscope and a Nikon D850 DSLR camera. Scanning electron microscopy (SEM) images were acquired using a FEI Quanta 650 FEG Scanning Electron Microscope, under a vacuum pressure of 2 mbar and currents of 600 μA with no primary beam filters. Fig. 2F was captured with a custom-made Large Field Detector (LFD) at a voltage of 10 kV; Fig. 2G was obtained with an Everhart-Thornley Detector (ETD) operating at a high voltage of 25.00 kV. Elemental maps were generated using a Bruker M4 Tornado micro X-Ray fluorescence (XRF) spectrometer instrument at Boyue Instrument (Shanghai) Co., Ltd., in Shanghai, China.

Reflectance transformation imaging is a technique that uses a series of images captured with different lighting directions with the position of the camera and specimens kept in a fixed position. These images are then combined in such a way that the orientation of the light source can be manipulated alongside other techniques that enhance the contrast of topographic features, such as the removal of color information and giving the surface a 'metallic quality' (specular enhancement). This method is particularly useful for weathered fossils, where color differences may provide misleading information regarding the topographic relationships of particular features. The RTI datasets were generated using a Broncolor Scope D50 and Canon R5 EOS camera with a 70mm F2.8 DG MACRO camera lens. Each dataset used a total of 48 images, that were subsequently processed using Relight (*35*) to create polynomial texture maps (PTMs). Camera settings used for each specimen are available in the supporting information. PTMs were subsequently visualized using RTI viewer (*36*) using the default rendering, diffuse gain, specular enhancement and normal visualization options. For specimens with substantial relief, multiple images at different focal planes were stacked using Photoshop, prior to PTM creation in relight. Full details of the imaging parameters used in each figure are given in Table S1 and lighting directions are shown in individual figure panels using an inset sphere.

Interpretative drawings were produced in Photoshop based on multiple images using different lighting directions and imaging modes to accurately convey all preserved morphological and topographical information relevant to the interpretation of the specimens.

Measurements of the diameters of the impressions of microvilli were collected from published images for a range of lophotrochozoan genera including annelids (*Platynereis* (*37*), *Siboglinum (38)*), Brachiopoda (*Macandrevia (38)*, *Discinisca (6)*) and molluscs (*Mopalia (28), Acanthochiton (13), Octopus* köllikers organ (*22*)). Microvillar tubules were measured in ImageJ and plots were generated using R.

Phylogenetic analyses made use of a previously published morphological character matrix compiled by some of the authors (*12*), which is derived from a number of previous studies aimed at understanding the interrelationships of early lophotrochozoans (*1, 14, 39*). Character scores for early fossil molluscs were updated to accommodate the unique combination of features observed in *Shishania aculeata.*

Phylogenetic analyses were performed using MrBayes 3.2.7 (*40*) using a dataset of early fossil and extant molluscs, brachiopods and annelids that has been successively added to over the course of a number of recent studies of extinct lophotrochozoans (*1, 12, 14, 39*). Changes to the character scores in this dataset, including justifications of scores for *Shishania aculeata* are included in the supplementary information. Ancestral state reconstructions were carried out in separate analyses where nodes of interests were constrained using monophyly constraints, but positions of taxa were otherwise allowed to vary, therefore incorporating a degree of phylogenetic uncertainty in our results. All analyses were performed with the mk + gamma model with a correction for scoring only parsimony informative characters. 100,000,000 generations were requested, with analyses stopping automatically once the average deviation of split frequencies was <0.01. Convergence was assessed using the PSRF and ESS scores calculated using the sump command in MrBayes. As in previous analyses of this dataset, analyses

were performed with and without topological constraits for the in-group relationships of annelids. Further analyses were performed excluding the controversial Ediacaran genus *Kimberella* to assess if its inclusion or exclusion impacted the phylogenetic position of *Shishania.*

Phylogenetic analysis and character scores

Our dataset is derived from the matrix of Guo, Parry, Vinther, Edgecombe, Wei, Zhao, Zhao, Béthoux, Lei and Chen (*12*) which was derived from a number of recent studies of early lophotrochozoan fossils (*1, 14, 39, 41-43*). We have implemented few changes to the previous version of this matrix and most are related to the coding of sclerites and chaetal homologs such that the coded characters more accurately reflect the diversity of morphology present in early fossil taxa and to incorporate the new combination of characters observed in *Shishania.* Changes to the previous matrix are outlined in the character descriptions below. For clarity characters that are new, have modified scores, character states or formulations are marked with an asterisk (*).

1. Spiral cleavage
    0 Absent
    1 Present

2. 4d mesentoblast
    0 Absent
    1 Present

3. Prototroch
    0 Absent
    1 Present

4. Metatroch
    0 Absent
    1 Present

5. Opposed band larval feeding
    0 Absent
    1 Present

6. Oral brush
    0 Absent
    1 Present

7. Ciliated region on episphere
    0 Absent
    1 Present

8. Type of ciliated region on episphere
    0 meniscotroch
    1 akrotroch

9. Ciliated food groove or adoral ciliary band
    0 Absent
    1 Present

10. Telotroch

0 Absent
1 Present

11. Neurotroch
0 Absent
1 Present

12. Apical tuft
0 Absent
1 Present

13. Apical cross
0 Absent
1 Present

14. Mitraria larva
0 Absent
1 Present

15. Hermaphroditism
0 Absent
1 Present

16. Acrosome
0 Absent
1 Present

17. Acrosomal tube
0 Absent
1 Present

18. Sperm mitochondrial interpolation
0 Absent
1 Present

19. Sperm flagellum
0 posterior
1 anterior
2 two

20. Posterior growth zone
0 Absent
1 Present

21. Cephalic tentacles
0 Absent
1 Present

22. Perioral tentacles
0 Absent
1 Present

23. Perioral tentacle position
    0 encircle mouth
    1 in arc around nuchal organ

24. Captacula
    0 Absent
    1 Present

25. Lophophore
    0 Absent
    1 Present

26. Lophophore origin
    0 Second pair of coelomic sacs, at metamorphosis
    1 Mid-trunk, prior to metamorphosis

27. Lophophore tentacle disposition
    0 Single side
    1 Both sides

28. Lophophore Tentacle rows per side in trocholophe stage
    0 No additional ablabial row
    1 Adlabial and ablabial row

29. Lophophore Tentacle rows per side in post-trocholophe stage
    0 No additional ablabial row
    1 Adlabial and ablabial row

30. Lophophore Median tentacle in early development
    0 Absent
    1 Present

31. Lophophore Site of tentacle addition
    0 At two points located behind the mouth
    1 At the tip of each lophophore arm

*32. Lophophore nerve ring forming accessory brachial nerve. This character should be inapplicable in molluscs, but was previously scored as absent. This has been corrected.
    0 forming ring (circumoral or inner nerve ring)
    1 forming accessory brachial nerve

33. Lophophore Musculature
    0 Outer main tentacle muscle; two pairs of inner longitudinal muscles
    1 Peripheral muscle fibres

34. Lophophore Forms closed loop
    0 Diverging laterally
    1 Closed loop

35. Lophophore Coiling direction

0 Anteriad
1 Posteriad

36. Lophophore Adjustor muscle
0 Absent
1 Present

37. Palps
0 Absent
1 Present

38. External palps
0 Absent
1 Present

39. Palp number
0 crown
1 pair
2 Owenia type crown
3 terebelliform type buccal tentacles

40. Buccal tentacles retractable
0 Absent
1 Present

41. Palp position
0 ventral
1 ventrolateral
2 lateral
3 forming branchial crown
4 dorsal
5 within the pharynx or mouth opening

42. Palp attachment
0 peristomial
1 prostomial
2 buccal cavity

43. Palp morphology
0 smooth
1 grooved
2 papillose
3 sensory palpodes

44. Biarticulate palps
0 Absent
1 Present

45. Palps with internal canal
0 Absent
1 Present

46. Commissure 1
    0 Absent
    1 Present

47. Commissure 2
    0 Absent
    1 Present

48. Commissure 3
    0 Absent
    1 Present

49. Commissure 4
    0 Absent
    1 Present

50. Commissure 5
    0 Absent
    1 Present

51. Commissure 6
    0 Absent
    1 Present

52. Commissure 7
    0 Absent
    1 Present

53. Commissure 8
    0 Absent
    1 Present

54. Commissure 9
    0 Absent
    1 Present

55. Commissure 10
    0 Absent
    1 Present

56. Commissure 11
    0 Absent
    1 Present

57. Commissure 12
    0 Absent
    1 Present

58. Commissures 4 and 5 fused
    0 Absent

1 Present

59. Commissures 6 and 7 fused
0 Absent
1 Present

60. Commissures 1 2 and 3 fused
0 Absent
1 Present

61. Terminal palpode
0 Absent
1 Present

62. Median antenna
0 Absent
1 Present

63. Position of median antenna
0 anterior
1 median
2 posterior

64. Lateral antennae
0 Absent
1 Present

65. Paired antennae morphologically similar to palps
0 Absent
1 Present

66. Eyes
0 Absent
1 Present

67. Multicellular adult eyes
0 Absent
1 Present

68. Unpigmented ciliary ocelli
0 Absent
1 Present

69. Light sensitive statocysts
0 Absent
1 Present

70. Ventral glandular area on anterior segments
0 Absent
1 Present

71. Nuchal commissure
    0 Absent
    1 Present

72. Cerebral commissures
    0 Absent
    1 Present

73. Commissural ganglion
    0 Absent
    1 Present

74. Dorsal ganglia
    0 Absent
    1 Present

75. Rectal commissure
    0 subrectal
    1 suprarectal

76. Ventral nervous system
    0 Absent
    1 Present

77. Ventral ganglion on CC
    0 Absent
    1 Present

78. Brain with multiple transverse commissures
    0 Absent
    1 Present

79. Corpora pedunculata
    0 Absent
    1 Present

80. Stomatogastric nerve ring
    0 Absent
    1 Present

81. Circumoral nerve ring
    0 Absent
    1 Present

82. Paired circumoral connectives
    0 Absent
    1 Present

83. Ventral nerve cord in mid body
    0 Absent
    1 Present

84. Median nerve in ventral nerve cord
    0 Absent
    1 Present

85. Single ventral neurite bundle
    0 Absent
    1 Present

86. Serially repeated ganglia
    0 Absent
    1 Present

87. Serially repeated segmental nerves
    0 Absent
    1 Present

88. Number of segmental nerves
    0 two
    1 three
    2 four
    3 five

89. Enlarged nerve associated with the parapodia or chaetae
    0 Absent
    1 Present

90. Supraesophageal or cerebral ganglion
    0 Absent
    1 Present

91. Brain cerebral ganglion subepithelial and internal
    0 Absent
    1 Present

92. Additional neurite bundles originating in brain
    0 Absent
    1 Present

93. Giant fibre system
    0 Absent
    1 Present

94. Giant fibres positioned ventrally
    0 Absent
    1 Present

95. More than two giant fibres
    0 Absent
    1 Present

96. Ventral nerve cords merging posterior of anterior segments
    0 Absent
    1 Present

97. Ventral cord within the epidermis
    0 subepidermal
    1 intraepidermal

98. Segmentally arranged commissures in VNC
    0 Absent
    1 Present

99. Nuchal organs
    0 Absent
    1 Present

100. Nuchal organ structure
    0 pits or grooves
    1 posterior projections
    2 caruncle
    3 internalised

101. Body shape
    0 dorsoventrally flattened
    1 vermiform
    2 laterally compressed
    3 vertical body with benthic lifestyle

102. Body dorsally shortened
    0 Absent
    1 Present

103. Body cylindrical
    0 Absent
    1 Present

104. Posterior elongation
    0 Absent
    1 Present

105. Anterior elongation
    0 Absent
    1 Present

106. Torsion
    0 Absent
    1 Present

107. Longitudinal muscle bands
    0 Absent
    1 Present

108. Circular muscles
0 Absent
1 Present

109. Circular muscles forming complete outer layer
0 Absent
1 Present

110. Paired coelomic cavities
0 Absent
1 Present

111. Serial repetition of coelomic compartments
0 Absent
1 Present

112. Co-ordinated serial repetition of multiple body parts
0 Absent
1 Present

113. Type of serialisation
0 oligomery
1 polymery

114. Pygidial cirri
0 Absent
1 Present

115. Pygidial cirri number
0 one pair
1 two or more pairs

116. Head differentiated into prostomium and peristomium
0 Absent
1 Present

117. Prostomium fused to peristomium
0 Absent
1 Present

118. Retractable head
0 Absent
1 Present

119. Anterior prostomial lobe
0 Absent
1 Present

120. Anterior body region made of circa eight or nine chaetigers
0 Absent

1 Present

121. Prostomium demarcated by distinct groove
0 Absent
1 Present

122. Prostomium annulated cone
0 Absent
1 Present

123. Shovel shaped prostomium
0 Absent
1 Present

124. Length width ration of shovel head
0 approx equal
1 elongate
2 wider than long

125. Peristomium
0 limited to lips
1 ring or rings

126. Peristomium ring number
0 one ring
1 two rings
2 rings and collar

127. Peristomial cirri
0 Absent
1 Present

128. Clitellum
0 Absent
1 Present

129. Mantle cavity
0 Absent
1 Present

130. Peripheral mantle cavity
0 Absent
1 Present

131. Mantle cavity restricted posterior
0 Absent
1 Present

132. Ctenidia
0 Absent
1 Present

133. Serial ctenidia
    0 Absent
    1 Present

134. Pairs of ctenidia
    0 one pair
    1 three or four pairs
    2 five pairs
    3 eight or more pairs

135. Ventral respiratory cavity
    0 Absent
    1 Present

136. location of gills relative to anus
    0 adanal
    1 abanal

137. Ventral ctenidia posterior only
    0 Absent
    1 Present

138. Gill morphology
    0 unipectinate
    1 bipectiate

139. Unpaired gills
    0 Absent
    1 Present

140. Branchiae
    0 Absent
    1 Present

141. Branchus type
    0 parapodial
    1 dorsal
    2 ctenidia

142. Parapodial gills interramal
    0 Absent
    1 Present

143. Dorsal gills Distribution
    0 Along body
    1 Restricted to anterior

144. Muscular foot
    0 Absent
    1 Present

145. Foot modified for digging
0 Absent
1 Present

146. Duogland system
0 Absent
1 Present

147. Caudal appendage
0 Absent
1 Present

148. Body with trunk and introvert
0 Absent
1 Present

149. Introvert longer than trunk
0 Absent
1 Present

150. Pedicle Presence
0 Absent
1 Present

151. Pedicle Constitution
0 Massive or uniform
1 Densely stacked tabular discs

152. Pedicle Biomineralization
0 Absent
1 Present

153. Pedicle Bulb
0 Absent
1 Present

154. Pedicle Distal rootlets
0 Absent
1 Present

155. Pedicle Tapering
0 Uniform thickness
1 Tapering

156. Pedicle Coelomic region
0 Absent
1 Present

157. Pedicle Surface ornament
0 Smooth

1 Regular annulations
2 Irregular wrinkles

158. Pedicle Nerve impression
0 Absent
1 Present

159. Serially repeated parapodia
0 Absent
1 Present

160. Anterior segments with cephalised cirri
0 Absent
1 Present

161. Segment 1 notopodia only
0 Absent
1 Present

162. Segment 1 elongated to form trunk
0 Absent
1 Present

163. Shape notopodia
0 prominent lobe
1 small lobes or chaetae only
2 notopodial ridges

164. Shape neuropodia
0 prominent lobe
1 small lobes or chaetae only

165. Enlarged neuropodia
0 Absent
1 Present

166. Tori
0 Absent
1 Present

167. Notopodial tori
0 Absent
1 Present

168. Neuropodial tori
0 Absent
1 Present

169. Lateral dorsal cirrus organs
0 Absent
1 Present

170. Dorsal organ
0 Absent
1 Present

171. Cirriform notopodia of anterior segments
0 Absent
1 Present

172. Dorsal cirri
0 Absent
1 Present

173. Dorsal cirri with alternating morphology
0 Absent
1 Present

174. Interruption of alternation at 4th segment
0 Absent
1 Present

175. Elytrae
0 Absent
1 Present

176. Elytrae on posterior segments
0 Absent
1 Present

177. Type of alternation
0 alternation of elytrae and cirri
1 alternation of elytron morphology

178. Ventral cirri
0 Absent
1 Present

179. Monociliate epidermal cells
0 Absent
1 Present

180. Ventral locomotory cillia
0 Absent
1 Present

181. With ciliated groove
0 Absent
1 Present

182. Annelid type cuticle made of layers of collagen fibres
0 Absent

1 Present

183. Rugose epidermis
0 Absent
1 Present

184. Epidermal papillae
0 Absent
1 Present

185. Dwelling tube
0 Absent
1 Present

186. Tube agglutinated
0 Absent
1 Present

187. Tube building organ
0 Absent
1 Present

188. Chitinous appendages secreted by microvilli
0 Absent
1 Present

189. Anal chaetal ring
0 Absent
1 Present

190. Posteriorly directed dorsal protective chaetae
0 Absent
1 Present

191. Segment 1 achaetous
0 Absent
1 Present

192. Chaetal inversion
0 Absent
1 Present

193. Chaetae in fascicles
0 Absent
1 Present

194. Serial repetition of chaetal bundles
0 Absent
1 Present

195. Number of serialised bundles

0 Oligomery
1 metamery

196. Chambered or camerate chaetae with internal diaphragms
0 absent
1 present

*197. Paleae or flattened chaetae/sclerites. The previous definition of this character encompassed only the paleae of annelids (e.g. Chrysopetalidae and the anterior chaetae of Pectinariidae) and *Wiwaxia.* It has been expanded here to include the flat sclerites of aculiferan molluscs.
0 Absent
1 Present

198. stalked chaetae or sclerites
0 absent
1 present

*199. Hollow sclerites or chaetae
The previous definition of this character conflated the presence of mineralisation and being hollow. Consequently, we have reformulated this character such that it scores only for chaetae that are solid, and mineralised chaetae are coded as a separate character (200, below). *Kulindroplax* and *Acaenoplax* are scored as uncertain for this character, and *Wiwaxia* is scored as absent, as the blade of the chaetae are solid and only the stalk is potentially hollow.
0 Absent
1 Present

200. Mineralised chaetae
0 Absent
1 Present

201. Longitudinal to spherulitic fibrous ultrastructure in sclerites
0 Absent
1 Present

202. Chaetae arranged in peripheral zones
0 Absent
1 Present

203. Protrusable retractable chaetae
0 Absent
1 Present

204. Chaetal distribution
0 dorsal and ventral
1 ventral only
2 dorsal only
3 restricted to gizzard

205. Dorsal chaetae in rows
0 Absent
1 Present

206. Ventral chaetae in rows
0 Absent
1 Present

207. External ventral chaetae
0 Absent
1 Present

208. External dorsal chaetae
0 Absent
1 Present

209. Chaetae on dorsal body wall
0 Absent
1 Present

210. Compound chaetae
0 Absent
1 Present

211. Compound position
0 neuropodial
1 neuro and notopodial

212. Ligaments
0 Absent
1 Present

213. Number of ligaments
0 one
1 two

214. Compound fold
0 Absent
1 Present

215. Capillary chaetae
0 Absent
1 Present

216. Noto capillaries
0 Absent
1 Present

217. Neuro capillaries
0 Absent
1 Present

218. Capillary chaetae restricted to anterior chaetigers
0 Absent
1 Present

219. Aciculae
0 Absent
1 Present

220. Notoaciculae
0 Absent
1 Present

221. Neuroaciculae
0 Absent
1 Present

222. Aciculae restricted to anterior segments
0 Absent
1 Present

223. Dentate hooks
0 Absent
1 Present

224. Long dentate hooks
0 Absent
1 Present

225. Uncini
0 Absent
1 Present

226. Hooks with beard
0 Absent
1 Present

227. Neuro hooks
0 Absent
1 Present

228. Noto hooks
0 Absent
1 Present

229. Falcate hooks
0 Absent
1 Present

230. Neuro falcate hooks
0 Absent
1 Present

231. Noto falcate hooks
0 Absent

1 Present

232. Hooks compound
0 Absent
1 Present

233. Hooded chaetae
0 Absent
1 Present

234. Fine silk notochaetae
0 Absent
1 Present

235. Chaetal basket
0 Absent
1 Present

236. Cuticular hooks
0 Absent
1 Present

237. Cuticular hooks in rings
0 Absent
1 Present

238. Scattered cuticular hooks
0 Absent
1 Present

*239. Nephridia. *Wiwaxia* was previously scored for this character in error and has been rescored as uncertain.
0 Absent
1 Present

240. Ciliophagocytal organ
0 Absent
1 Present

241. Serially repeated nephridia
0 Absent
1 Present

242. Distribution of nephridia
0 in most segments
1 anterior sterile nephridia and posterior gonoducts
2 one pair of anterior nephridia

243. Adult nephridia
0 Absent
1 Present

244. Adult nephridia type
0 protonephridia
1 metanephridia

245. Head kidneys
0 Absent
1 Present

246. Head kidney type
0 protonephridia
1 metanephridia

247. Gonoducts
0 nephridial/coelomoducts
1 separate from coelomoducts

248. Metanephridial duct
0 Absent
1 Present

249. Terminal cell
0 Absent
1 Present

250. Filter of terminal cells with clefts
0 Absent
1 Present

251. Microvillar filter
0 Absent
1 Present

252. Nephridial podocyte lining
0 Absent
1 Present

253. Metanephridial mantle cell
0 Absent
1 Present

254. Complete through gut
0 Absent
1 Present

255. Through gut shape
0 following AP axis
1 U-shape

256. Straight gut coiled or folded
0 Absent
1 Present

257. U- shape gut position of anus
0 anterior
1 anteroterminal inside lophophore
2 anteroterminal outside lophophore

258. Proboscis surrounded by rhynchocoel
0 Absent
1 Present

259. Gut with side branches
0 Absent
1 Present

260. Helical coiling of gut
0 Absent
1 Present

261. Buccal organ or pharynx
0 Absent or occluded
1 Present

262. Buccal organ position
0 Absent
1 axial
2 ventral
3 dorsal

263. Buccal organ muscular
0 Absent
1 Present

264. Pharynx eversible
0 Absent
1 Present

265. Proboscis papillae
0 Absent
1 Present

266. Ciliated pharynx
0 Absent
1 Present

267. Pharynx with cuticular ridges
0 Absent
1 Present

268. Gular membrane
0 Absent
1 Present

269. Proventricle
0 Absent
1 Present

270. Jaws
0 Absent
1 Present

271. Jaw growth by shedding
0 Absent
1 Present

272. Jaw growth by accretion
0 Absent
1 Present

273. Jaw type
0 dorso ventral
1 lateral
2 trepan
3 terminal ring
4 with mandibles and maxillae

274. Venom gland
0 Absent
1 Present

275. Number of jaw elements per side
0 unequal
1 equal

276. Jaw element size asymmetry
0 Absent
1 Present

277. Right MIII element
0 Absent
1 Present

278. Eunicidan jaw type
0 ctenognath
1 symmetrognath
2 prionognath
3 labidognath

279. Calcified mandibles
0 Absent
1 Present

280. Dorsal carriers

0 Absent
1 Present

281. Ventral carrier
0 Absent
1 Present

282. MI Articulation
0 Absent
1 Present

283. Radula
0 Absent
1 Present

284. Number of tooth rows
0 few rows
1 many rows
2 a single row

285. Median tooth
0 Absent
1 Present

286. Multiple lateral and marginal teeth
0 Absent
1 Present

287. Radula dentition
0 homodont
1 heterodont

288. Dorsolateral folds
0 Absent
1 Present

289. Closed circulation
0 Absent
1 Present

290. Heart body
0 Absent
1 Present

291. Respiratory pigment
0 Haemoglobin
1 Chlorocruin
2 Hemerythrin

292. Shell plates or sclerites with continual accretionary growth
0 Absent

1 Present

293. Sclerites penetrated by chaetal pores
0 Absent
1 Present

294. S1 or ventral bilateral sclerite
0 Absent
1 Present

295. S2 or dorsal bilateral sclerite
0 Absent
1 Present

296. Opposing bilterally sclerites forming bivalved scleritome
0 Absent
1 Present

297. Bivalved sclerites Hinge line shape
0 Astrophic
1 Strophic

298. Sclerites forming closed filtration chamber
0 Absent
1 Present

299. Bivalved sclerites Commissure Exact correspondence of valve margins
0 Margins align exactly when valves closed
1 Margins of different shape or size

300. Bivalved sclerites Commissure Sulcate
0 Rectimarginate
1 Uniplicate
2 Sulcate

301. Bivalved sclerites Commissure Circular
0 Continuous round outline with no corners (except at the hinge);
1 Lateral margins linear

302. Bivalved sclerites Commissure Lateral margins
0 Subparallel
1 Diverging
2 Initially diverging, becoming subparallel

303. Bivalved sclerites Apophyses
0 Absent
1 Present

304. Bivalved sclerites Apophyses Morphology
0 Deltidiodont
1 Cyrtomatodont

2 Pseudodont

305. Bivalved sclerites Apophyses Dental plates
0 Absent
1 Present

306. Bivalved sclerites Sockets
0 Absent
1 Present

307. Bivalved sclerites Socket ridges
0 Absent
1 Present

308. Bivalved sclerites muscle scars Ventral
0 Absent
1 Present

309. Bivalved sclerites muscle scars Ventral: Position
0 Posterolateral and medial attachments
1 Medial attachments only

310. Bivalved sclerites muscle scars Adjustor
0 Absent
1 Present

311. Bivalved sclerites muscle scars Dorsal adductors
0 Dispersed
1 Radially arranged
2 Quadripartite

312. Bivalved sclerites muscle scars Adductors: Position
0 Oblique
1 At high angle

313. Bivalved sclerites muscle scars Dermal muscles
0 Absent or weakly developed
1 Strongly developed

314. Bivalved sclerites muscle scars unpaired median (levator ani)
0 Absent
1 Present

315. Bivalved sclerites muscle scars Dorsal diductor
0 Absent
1 Present

316. Bivalved sclerites muscle scars Dorsal diductor: Position
0 Close to commissural plane
1 Oblique to commissural plane
2 At high angle to commissural plane

317. Dorsal valve Growth direction
0 Holoperipheral
1 Mixoperipheral
2 Hemiperipheral

318. Dorsal valve posterior surface: Differentiated
0 Posterior face of dorsal valve not differentiated
1 Posterior face of dorsal valve forms distinct cardinal area or pseudointerarea

319. Dorsal valve Differentiated posterior surface: Morphology
0 Curved lateral profile
1 Planar lateral profile

320. Dorsal valve posterior surface: Medial groove
0 Absent
1 Present

321. Dorsal valve posterior surface: Notothyrium
0 Absent
1 Present

322. Dorsal valve posterior surface: Notothyrium: Shape
0 Parallel-sided cleft
1 Triangular

323. Dorsal valve posterior surface: Notothyrium: Chilidial plates
0 Open
1 Covered by chilidial plates

324. Dorsal valve Notothyrial platform
0 Absent
1 Present

325. Dorsal valve Medial septum
0 Absent
1 Present

326. Dorsal valve Cardinal shield
0 Absent
1 Present

327. Dorsal valve Cardinal processes
0 Absent
1 Present

328. Ventral valve growth direction
0 Holoperipheral
1 Mixoperipheral
2 Hemiperipheral

329. Ventral valve relative size
    0 Ventral valve markedly larger than Dorsal valve (ventribiconvex)
    1 Equivalve (subequally biconvex)
    2 Dorsal valve markedly larger than ventral valve (dorsibiconvex)

330. Ventral valve posterior surface: Differentiated
    0 posterior surface of shell not differentiated
    1 posterior surface of shell forms distinct cardinal area or pseudointerarea

331. Ventral valve posterior margin growth direction
    0 Inward-growing
    1 Outward-growing

332. Ventral valve posterior surface: Planar
    0 Curved lateral profile
    1 Planar lateral profile

333. Ventral valve posterior surface: Extent
    0 Low: Wider than deep
    1 High: Deeper than wide

334. Ventral valve posterior surface: Delthyrium
    0 Absent
    1 Present

335. Ventral valve posterior surface: Delthyrium: Shape
    0 Parallel sided
    1 Triangular
    2 Round

336. Ventral valve posterior surface: Delthyrium: Shape: Aspect of rounded opening
    0 Elongate: oval to rhombic
    1 Essentially circular
    2 Wider than long

337. Ventral valve posterior surface: Delthyrium: Cover
    0 Open
    1 Covered, at least in part

338. Ventral valve posterior surface: Delthyrium: Cover: Extent
    0 Covered only partially; partially open
    1 Completely covered

339. Ventral valve posterior surface: Delthyrium: Cover: Identity
    0 Pseudodeltidium
    1 Deltidial plate(s)
    2 Continuation of shell

340. Ventral valve posterior surface: Delthyrium: Pseudodeltidium: Shape
    0 Concave
    1 Convex

341. Ventral valve posterior surface: Delthyrium: Pseudodeltidium: Hinge furrows
    0 Absent
    1 Present

342. Ventral valve Umbonal perforation
    0 Umbo imperforate
    1 Umbonal perforation

343. Ventral valve Umbonal perforation: Shape
    0 Circular (or subcircular)
    1 Rhombic to oval
    2 Arising through decollation

344. Ventral valve Colleplax, cicatrix or pedicle sheath
    0 Absent
    1 Present

345. Ventral valve Median septum
    0 Absent
    1 Present

346. Sclerite ornament shell-penetrating spines
    0 Absent
    1 Present

347. Calcium Phosphate biomineralisation
    0 Absent
    1 Present

348. Calcium carbonate biomineralisation
    0 Absent
    1 Present

349. Calcium carbonate polymorph
    0 Calcite
    1 Aragonite

350. Sclerite periostracum flexibility
    0 Flexible
    1 Inflexible

351. Sclerite deposition with alternation of dense and porous layers
    0 Absent
    1 Present

352. Shell microstructure with fibrous bundles
    0 Absent
    1 Present

353. Tabular laminar secondary layer

0 Absent
1 Present

354. Laminated or stratiform shell microstructure
0 Absent
1 Present

355. Inner and outer laminae enclosing medial void
0 Absent
1 Present

356. bio
0 Lamellae not expressed at surface
1 Lamellae correspond to external shell ornament

357. Laminae at shell surface forming prominent regularly spaced ribs
0 Absent
1 Present

358. Co-marginal ribs ornamented with tubercles or pustules
0 Absent
1 Present

359. Fine growth increments between comarginal ribs
0 Absent
1 Present

360. Sclerite structure Stratiform laminae separated
0 Contiguous stratified layer
1 Laminae separated by organic layers or voids

361. Laminar microstructure with columns
0 Absent
1 Present

362. Sclerite stratiform laminae with polygonal ornament
0 Absent
1 Present

363. Sclerite canals
0 Absent
1 Present

364. Sclerite punctae
0 Absent
1 Present

365. Sclerite pseudopunctae
0 Absent
1 Present

366. Sclerite growth by marginal accretion
0 Absent
1 Present

367. Sclerite growth by subapical and internal accretion
0 Absent
1 Present

368. Sclerites with pointed apices
0 Absent
1 Present

369. Sclerites with Irregular apical surfaces
0 Absent
1 Present

370. Asymmetrical sclerite morphs
0 Absent
1 Present

371. Two forms of asymmetrical sclerite (mitral B and sellate C)
0 Absent
1 Present

372. Saddle shaped sellate sclerite
0 Absent
1 Present

373. Quadrate C or mitral type sclerite
0 Absent
1 Present

374. Mitral sclerites with plicae
0 Absent
1 Present

375. Bilaterally symmetrical sclerites with multiple shell apices
0 Absent
1 Present

376. Continuous variation between sclerite morphologies
0 Absent
1 Present

377. Serial repetition of self-similar sclerites
0 Absent
1 Present

378. Marginal setal fringe at aperture
0 Absent
1 Present

379. Setal fringe forming pseudosiphon
0 Absent
1 Present

380. Serial muscle scars on shell
0 Absent
1 Present

381. Byssus
0 Absent
1 Present

382. Byssal gape
0 Absent
1 Present

383. Auricles
0 Absent
1 Present

384. Anterior adductor scars
0 Absent
1 Present

385. Anterior adductor reduced
0 Absent
1 Present

386. Posterior adductor
0 Absent
1 Present

387. Posterior adductor reduced relative to anterior
0 Absent
1 Present

388. Position of posterior pedal retractor
0 anterodorsal
1 inset on the anterior

389. Pallial line
0 Absent
1 Present

390. Pallial sinus
0 Absent
1 Present

391. External ligament
0 Absent

1 Present

392. Ligament position
0 amphidetic
1 opisthodetic

393. Ligament type
0 simple
1 dupinvicular
2 alivincular
3 transverse
4 parivincular

394. Umbo
0 orthogyrous
1 prosogyrous
2 opisthogyrous

395. Hinge teeth
0 Absent
1 Present

396. Hinge tooth row
0 Absent
1 Present

397. Hinge tooth row gap
0 Absent
1 Present

398. Secondary teeth
0 Absent
1 Present

399. Cardinal hinge teeth
0 Absent
1 Present

400. Anterolateral hinge teeth
0 Absent
1 Present

401. Posterior lateral hinge teeth
0 Absent
1 Present

402. Ventral mantle fusion
0 Absent
1 Present

403. Parapodial shell plates

0 Absent
1 Present

404. Outer shell plates
0 Absent
1 Present

405. Inner shell plates attached by tongue and groove hinge
0 Absent
1 Present

406. Elytrae or plates enclosing body
0 Absent
1 Present

407. Prominent concentric rugae
0 Absent
1 Present

408. Folding inner shell plates
0 Absent
1 Present

409. Ventro lateral displacement of outer shell plates
0 Absent
1 Present

410. Tongue and groove articulation between shell plates
0 Absent
1 Present

411. Alternating articulation
0 Absent
1 Present

412. Differentiated anterior shell plates
0 Absent
1 Present

413. Number of differentiated anterior plates
0 one
1 two

414. Discrete muscle attachment scars on parapodial shell plates
0 Absent
1 Present

415. Type of non-accreting margin on parapodial shell plate
0 with onlapping of rugae
1 sharp termination of rugae

416. Dorsal depression between inner shell plates
0 Absent
1 Present

417. Number of inflections on outer shell plate
0 one
1 two
2 three
3 four

418. Number of inflections on inner plate
0 one
1 two
2 three
3 four
4 five

419. Fine denticles on non-accreting plate margin
0 Absent
1 Present

420. Medial depression on outer plate
0 Absent
1 Present

421. Left right asymetry in parapodial plates
0 Absent
1 Present

422. Brephic shell Embryonic shell
0 Absent
1 Present

423. Brephic shell morphology
0 Flat, disc-like (cf. Micrina)
1 Three prominent lobes forming a Y (cf. Paterimitra)
2 Spherical
3 Fusiform

424. Brephic shell Embryonic shell extended in larvae
0 Not extended; embryonic shell contiguous with adult shell
1 Extended into larval shell, separated from adult shell by prominent nick

425. Brephic shell Surface ornament
0 Smooth
1 Rounded pits
2 Polygonal impressions
3 Pustulose

426. Brephic shell Larval attachment structure
0 Without evidence of pedicle

1 With evidence of pedicle

427. Brephic shell Setulose
0 No evidence of setae in embryonic shell
1 Setae Present

428. Brephic shell Setal sacs
0 Absent
1 Present

429. Brephic shell Setal sacs: Number
0 One pair
1 Two pairs
2 Three pairs

430. Mantle canals Presence
0 Absent
1 Present

431. Mantle canals Morphology
0 Pinnate (=lemniscate)
1 Bifurcate
2 Baculate
3 Saccate

432. Mantle canals vascula lateralia
0 Absent
1 Present

433. Mantle canals vascula media
0 Absent
1 Present (in Dorsal valve)

434. Mantle canals vascula terminalia
0 Exclusively marginal (peripheral)
1 Directed peripherally and (intero) medially

435. Sclerites or shells enveloping the body
0 Absent
1 Present

436. Enveloping sclerites forming tube
0 Absent
1 Present

437. Pegma
0 Absent
1 Present

438. Protoconch
0 Absent

1 Present

439. Protoconch dorsal of tubular shell
0 Absent
1 Present

440. Anterior placed head plate
0 Absent
1 Present

441. Posteriorly placed tail valve
0 Absent
1 Present

442. Serially repeated median shell fields
0 Absent
1 Present

443. Intermediate shell plates
0 Absent
1 Present

444. Differentiated shell fields in intermediate plates
0 Absent
1 Present

445. Lateral division of intermediate shell plates
0 Absent
1 Present

446. Number of intermediate shell fields
0 five
1 six

447. Aesthete canal system
0 Absent
1 Present

448. Sclerites with aesthete canal system
0 Absent
1 Present

449. Shell plate with aesthete canal system
0 Absent
1 Present

450. Tunnels
0 Absent
1 Present

451. Number of tunnels

0 one
1 two

452. Articulamentum
0 Absent
1 Present

453. Sutural laminae apophyses
0 Absent
1 Present

454. Insertion plate
0 Absent
1 Present

455. Slitted insertion plates
0 Absent
1 Present

456. Type of slitted plates
0 cluster of small slits
1 one single slit

457. Pectinated insertion plates
0 Absent
1 Present

458. Length of apical area
0 less than 10% valve length
1 more than 10% of valve length

459. Growth style anterior plate
0 holoperipheral
1 mixoperipheral or hemiperipheral

460. Primary growth margin of head valve
0 anterior
1 posterior

461. Length width ratio of anterior plate
0 elongate
1 equal to subequal
2 transverse

462. Posterior margin of anterior plate
0 concave
1 sub linear
2 convex

463. Growth style of tail valve
0 holoperipheral

1 mixoperipheral or hemiperipheral

464. Length width ratio of tail valve
0 elongate
1 equal to subequal
2 transverse

465. Anterior margin of tail valve
0 concave
1 sublinear
2 convex

466. Intermediate valve growth style
0 holoperipheral
1 mixoperipheral or hemiperipheral

467. Length width ratio central row
0 elongate
1 equal or subequal
2 elongate

468. Anterior margin central row
0 concave
1 linear
2 convex

469. Posterior margin central row
0 concave
1 linear
2 convex

470. Apical angle central row
0 less 90 degrees
1 more 90 degrees

471. Coiled shell
0 Absent
1 Present

472. Coiling direction
0 exogastric
1 endogastric

473. Type of coiling
0 planispiral
1 dextral

474. Stromboid notch
0 Absent
1 Present

475. Siphonal notch
0 Absent
1 Present

476. Ventral suture
0 Absent
1 Present

477. Left and right shells with hinge
0 Absent
1 Present

478. Curved ventral shell margin
0 Absent
1 Present

479. Posterior mantle opening in shell
0 Absent
1 Present

480. Operculum
0 Absent
1 Present

481. Operculum in adult
0 Absent
1 Present

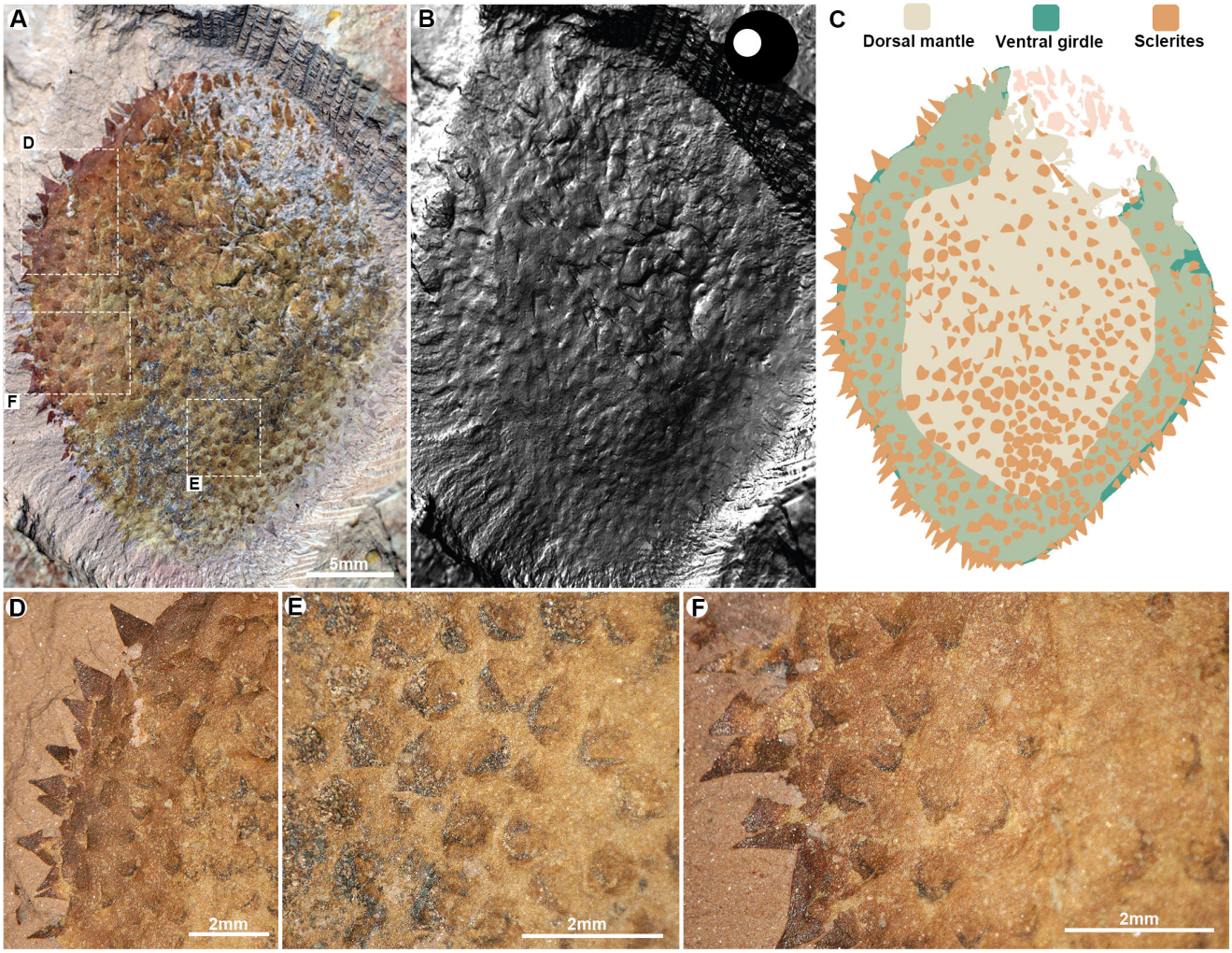

Fig. S1. Additional details of the holotype specimen YKLP 11500. (**A**) The image taken under normal light. (**B**) A Reflectance Transformation Imaging (RTI) photograph revealing the three-dimensional undulation of the dorsal surface that indicates regionalization of the body. (**C**) Interpretive illustration of the area highlighted in (B), emphasizing the separation of the ventral girdle from the remainder of the ventral surface. (**D**) Detail of sclerites along the lateral side of the animal's body. (**E**) Sclerites on the dorsal aspect of the animal, exhibiting a rounded cross base. (**F**) Sclerites in a range of orientations.

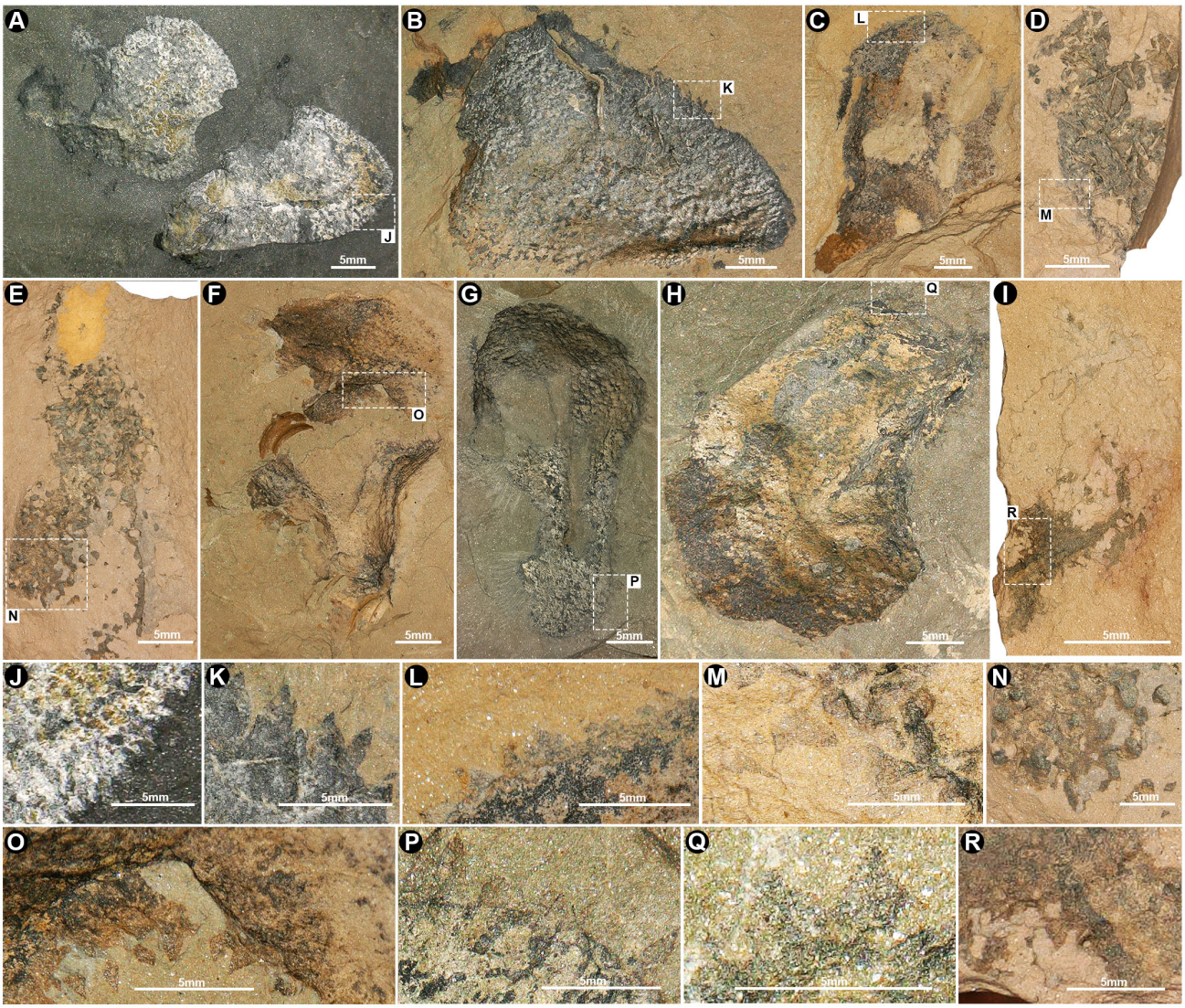

Fig. S2. Incomplete/poorly preserved specimens and sclerite details. (**A**) YKLP 11529a (part), preservation of two separate individuals in dorsal view. (**B**) YKLP 11530a (part), preservation of one individual with fewer characteristics. (**C**) YKLP 11531a (part), an incomplete specimen in dorsal view. (**D**) YKLP 11536, an incomplete specimen. (**E**) YKLP 11532, an incomplete specimen. (**F**) YKLP 11533, preservation of two incomplete individuals. (**G**) YKLP 11528, a complete individual in dorsal view. (**H**) YKLP 11534, a complete individual in dorsal view. (**I**) YKLP 11537a (part), an incomplete individual. (**J**) Sclerite magnification from (A). (**K**) Sclerite magnification from (B). (**L**) A close-up of sclerites from (C). (**M**) A close-up of sclerites from (D). (**N**) A close-up of sclerites from (E). (**O**) A close-up of sclerites from (F). (**P**) A close-up of sclerites from (G). (**Q**) A close-up of sclerites from (H). (**R**) A close-up of sclerites from (I). Scale bars for (A-I) are 5 mm, while scale bars for (J-R) are 2 mm.

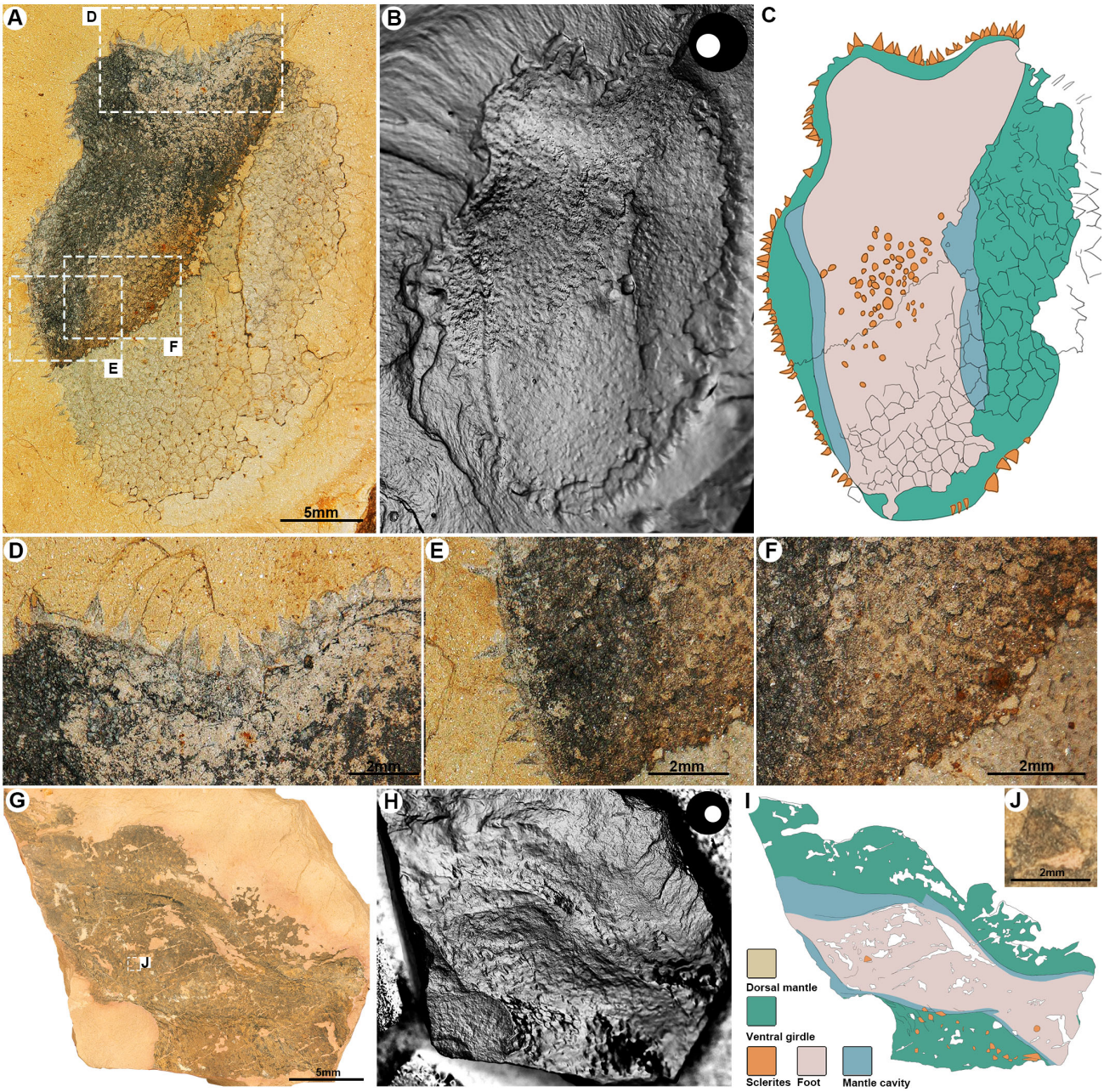

Fig. S3. Specimens showing ventral views of the foot, girdle and sclerites. (**A** to **F**) YKLP 11535, a complete specimen displaying a ventral view with color variation due to differentiation weathering. In (A), the image taken under normal light. In (B), an RTI image using specular enhancement, illustrating differences between the differentiation of the ventral surface into a foot and girdle. In (C), interpretive illustration based on (A) and (B), highlighting the foot. In (D), a close-up of the sclerites at the anterior margin shown in (A). In (E), a close-up of the sclerites at the left margin shown in (A). In (F), a close-up of the central sclerites from the dorsal side shown in (A). (**G** to **J**) YKLP 11505, incomplete specimen in ventral view. In (G), the image taken under normal light. In (H), an RTI image using specular enhancement, showcasing the three-dimensional structure of the midbody and

differentiation of the ventral region. In (I), an interpretive illustration based on (G) and (H). In (J), a close-up of a sclerite shown in (G) and (I).

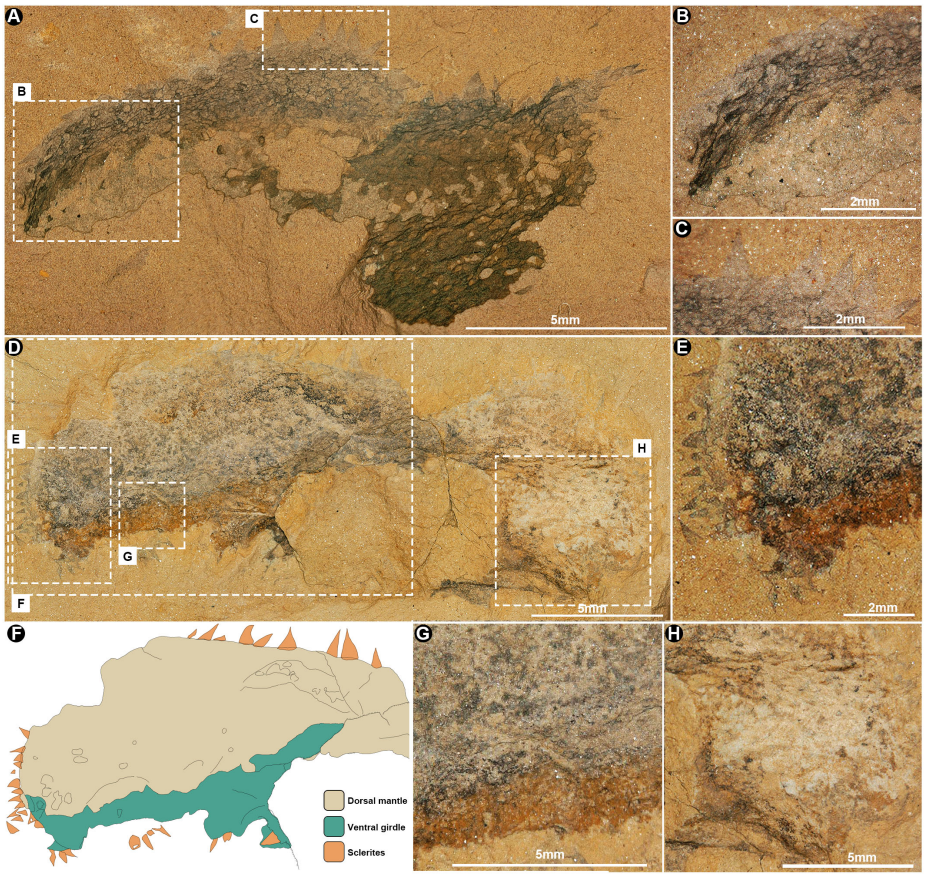

Fig. S4. Incomplete specimens in oblique/lateral view. (A) YKLP 11503, incomplete specimen in lateral/oblique view. (**B**) Detail of the presumed posterior, with sclerite tips oriented towards the posterior. (**C**) Detail of midbody sclerites oriented dorsally. (**D**) YKLP 11526, incomplete specimen in lateral/oblique view. (**E**) Detail of the sclerites and dorsal mantle in the posterior region. (**F**) An interpretive illustration based on the anterior region of (D). (**G**) A close-up of the lower part, highlighting distinct color differences separating the dorsal and ventral mantle. (**H**) A close-up of the posterior.

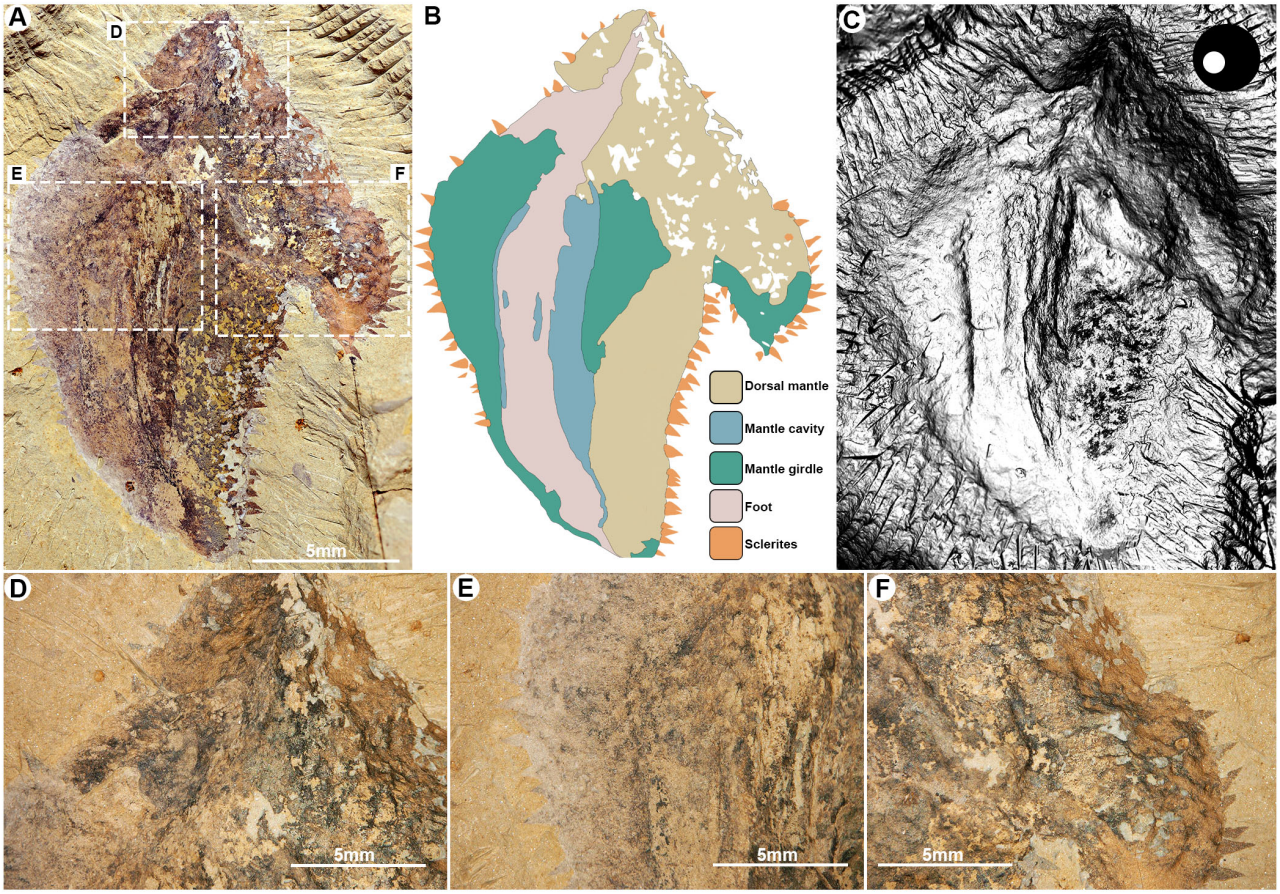

Fig. S5. YKLP 11527, a distorted/twisted specimen. (**A**) The complete specimen, exhibiting a distorted and twisted shape. (**B**) An interpretive illustration highlighting the major body regions. (**C**) An RTI image rendered using specular enhancement. (**D**) A close-up of the upper part, showing a contrast between the smooth left side and the right side with sclerites. (**E**) A close-up of the lower part, emphasizing the margins with sclerites and lighter colors. F, Magnification of the lower right part, highlighting the margins with sclerites and darker colors.

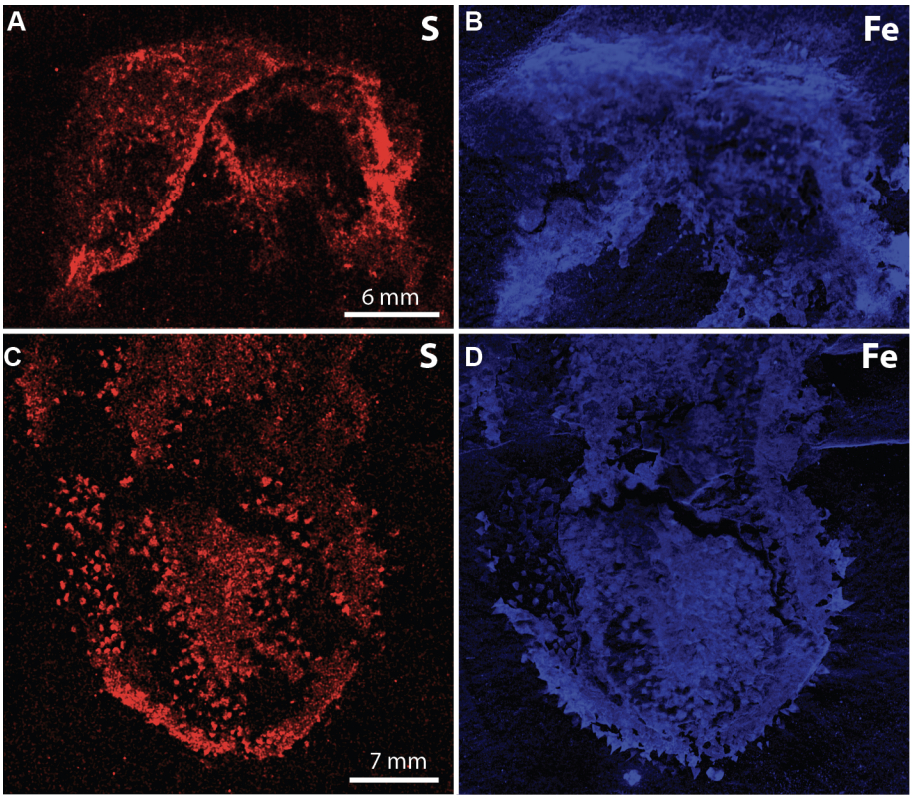

Fig. S6. Elemental maps of Fe and S of specimens shown in the main text figures. (**A** and **B**) Specimen YKLP 11502, elemental map for sulfur in (A) and iron in (B). (**C** and **D**) Specimen YKLP 11501, elemental map for sulfur in (C) and iron in (D).

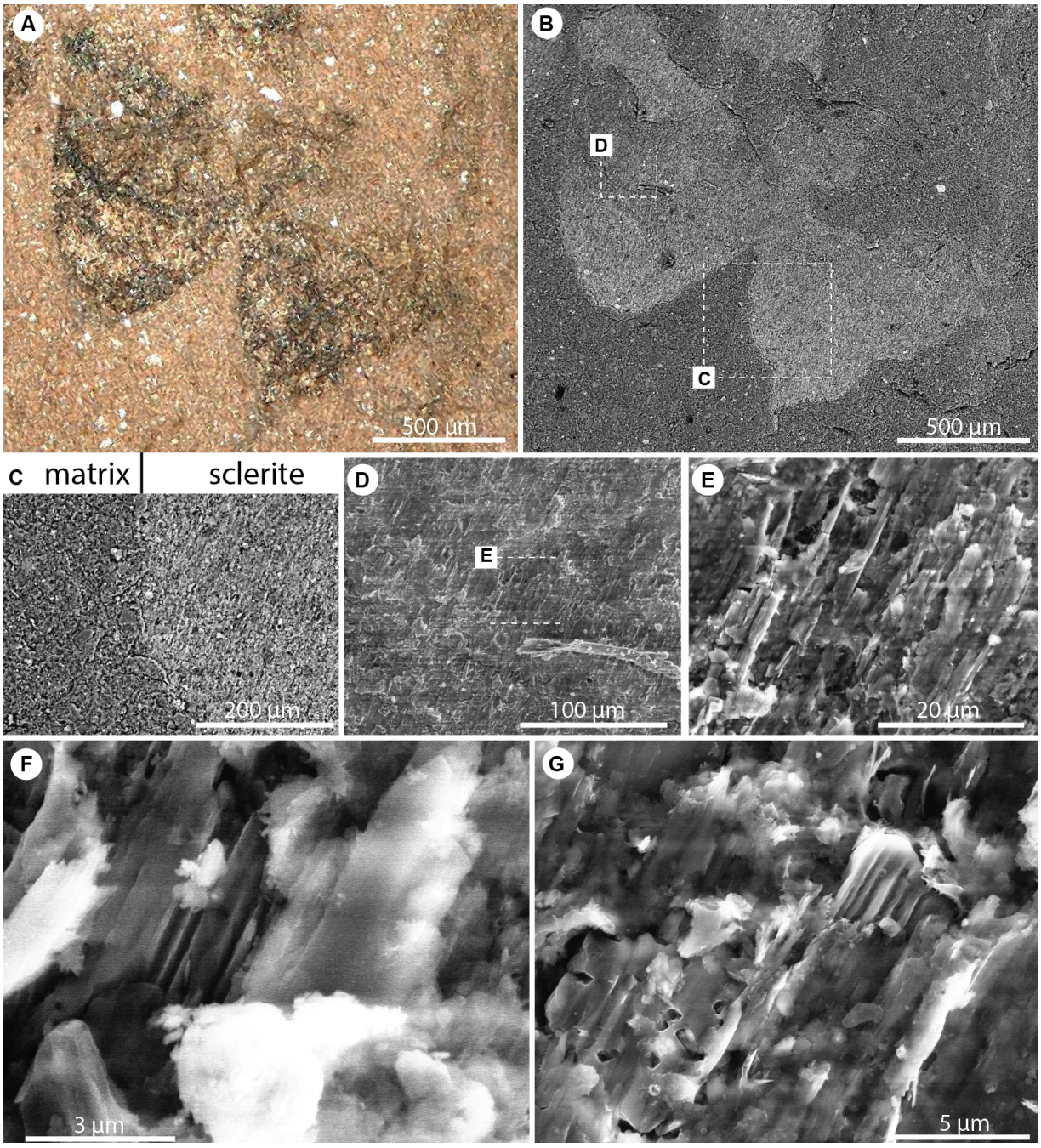

Fig. S7. Details of sclerite microstructure from specimen YKLP 11501. (**A**) Detail of sclerites, image taken under normal light by microscope. (**B**) Scanning Electron Microscope (SEM) image of the same area as in (A). (**C**) SEM image distinguishing the boundaries and microstructural differences between the matrix and the sclerites. (**D**) Microstructure details of the sclerites showing longitudinal fabric of longitudinal tubules. (**E**) Fabric of longitudinal tubules within the sclerites. (**F** and **G**) Detail of striations showing longitudinal cavities.

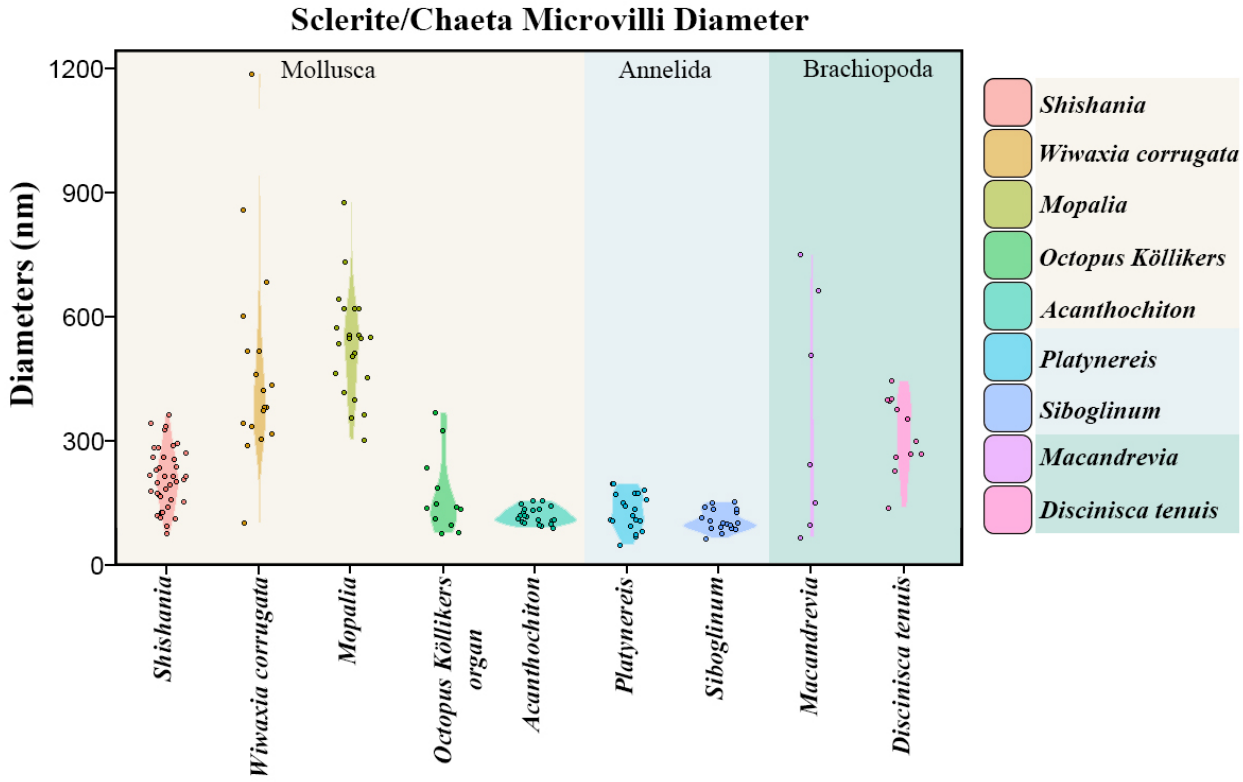

Fig. S8. Diameter of microvilli impressions from across Trochozoa. All measurements are the diameters of the cross sections of the impressions of microvilli from a range of taxa within Trochozoa. See the methods for details for the sources for individual taxa.

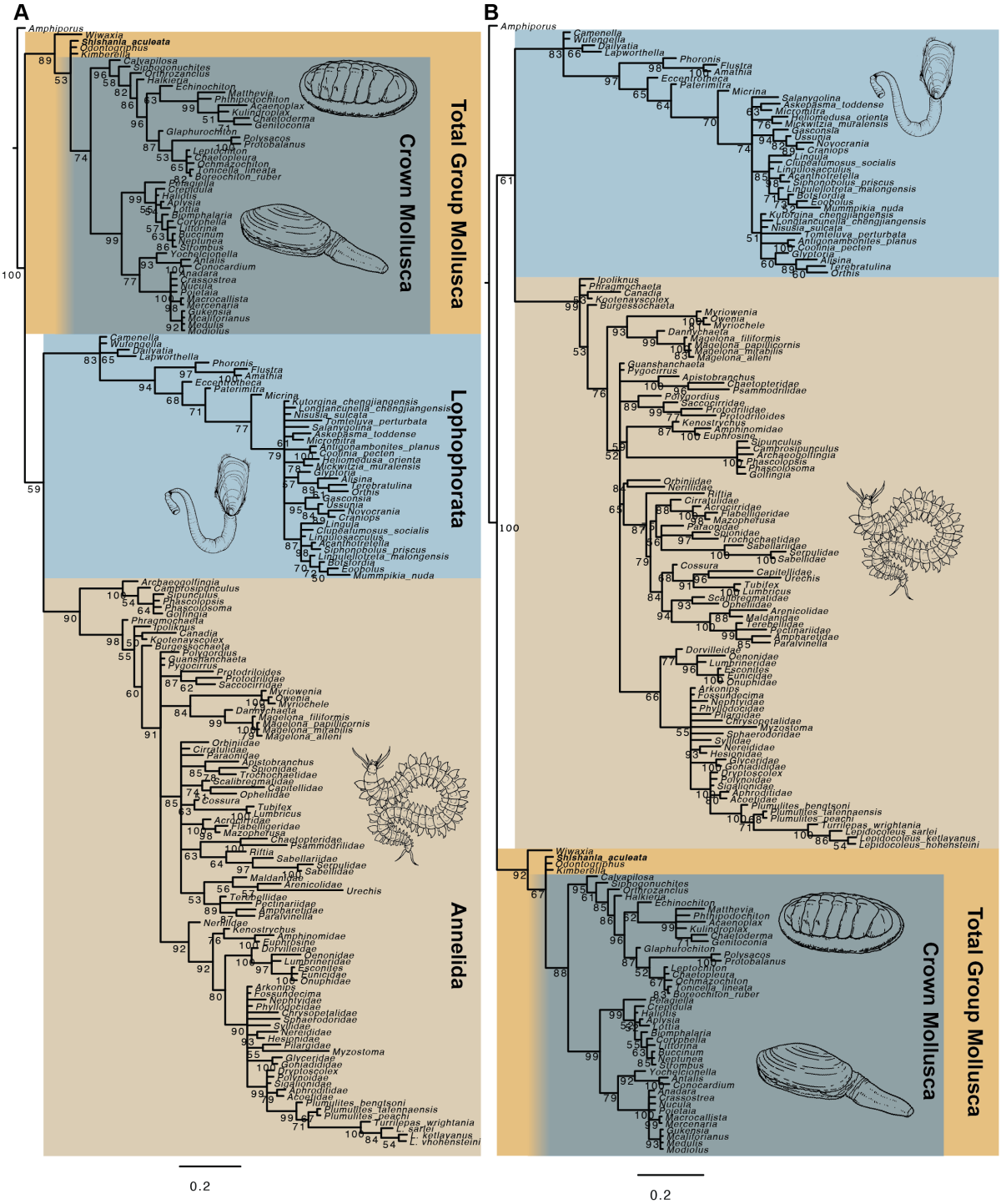

Fig. S9. Full results of phylogenetic analysis including the controversial Ediacaran taxon *Kimberella*. (**A**) Analysis with no topological constraints. (**B**) Analysis constraining the in-group relationships of annelids.

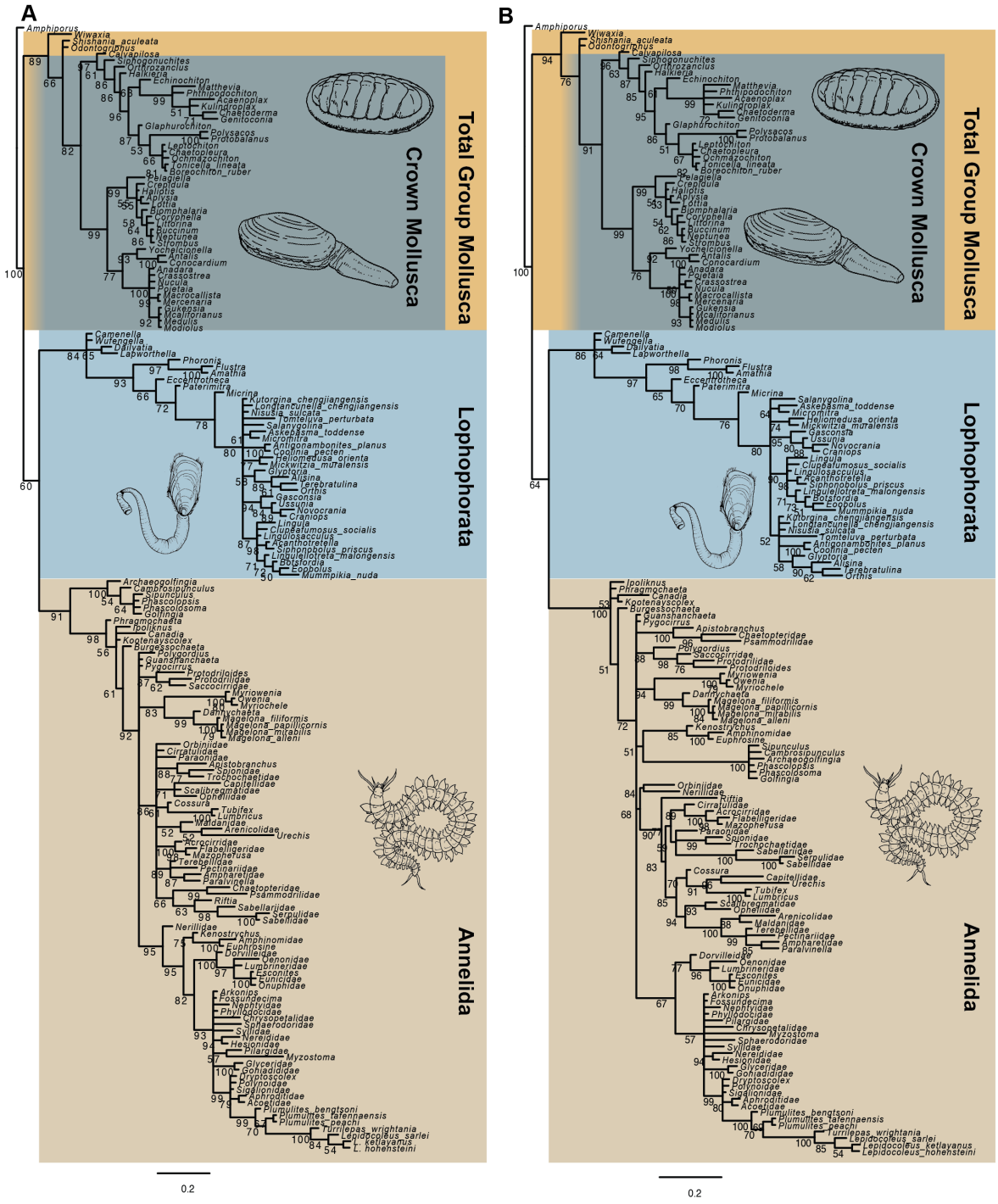

Fig. S10. Full results of phylogenetic analysis excluding the controversial Ediacaran taxon *Kimberella*. (**A**) Analysis with no topological constraints. (**B**) Analysis constraining the in-group relationships of annelids. Nodes are posterior probabilities, and topology shown is from the unconstrained analysis without *Kimberella.* Scale bar is in units of the expected number of substitutions per site.

Table S1.

Figure	Item	File	Rendering mode	Light Source Coordinates		Specular Enhancement settings			Gain for diffuse gain	
				x	y	Diffuse color	Specularity	Highlight size	Gain	Environment
Fig. 1	A		Normal unsharp masking	na	na	na	na	na	24.812	21.0526
	B		Specular enhancement	0.07	0.26	0	70	50	na	na
Fig. 3	A		Diffuse gain	-0.44	-0.11	na	na	na	11.111	na
	B		Specular enhancement	-0.21	-0.3	0	50	27	na	na
	G		Diffuse gain	0.39	-0.37	na	na	na	11.111	na
	H		Specular enhancement	-0.08	-0.11	0	47	48	na	na
Extended Data Figures										
Extended Data figure. 1										
	B		Specular enhancement	0.07	0.26	0	70	50	na	na
Extended Data figure. 3										
	B		Specular enhancement	0.11	-0.22	0	54	75	na	na
	H		Specular enhancement	0.46	-0.07	0	64	75	na	na
Extended Data figure. 5	C		Specular enhancement	-0.27	-0.18	0	70	70	na	na

Table S1: RTI Extract Settings used to produce figured images.